

ARTICLE

Drosophila FGF cleavage is required for efficient intracellular sorting and intercellular dispersal

Alex Sohr¹, Lijuan Du¹, Ruofan Wang¹, Li Lin², and Sougata Roy¹ 

How morphogenetic signals are prepared for intercellular dispersal and signaling is fundamental to the understanding of tissue morphogenesis. We discovered an intracellular mechanism that prepares *Drosophila melanogaster* FGF Branchless (Bnl) for cytoneme-mediated intercellular dispersal during the development of the larval Air-Sac-Primordium (ASP). Wing-disc cells express Bnl as a proprotein that is cleaved by Furin1 in the Golgi. Truncated Bnl sorts asymmetrically to the basal surface, where it is received by cytonemes that extend from the recipient ASP cells. Uncleavable mutant Bnl has signaling activity but is mistargeted to the apical side, reducing its bioavailability. Since Bnl signaling levels feedback control cytoneme production in the ASP, the reduced availability of mutant Bnl on the source basal surface decreases ASP cytoneme numbers, leading to a reduced range of signal/signaling gradient and impaired ASP growth. Thus, enzymatic cleavage ensures polarized intracellular sorting and availability of Bnl to its signaling site, thereby determining its tissue-specific intercellular dispersal and signaling range.

Introduction

Intercellular communication mediated by signaling proteins is essential for coordinating cellular functions during tissue morphogenesis. Owing to decades of research, the core pathways of developmental signaling and their roles and modes of action in diverse morphogenetic contexts are well characterized. We now know that a small set of conserved paracrine signals is universally required for most developing tissues and organs. These signals are produced in a restricted group of cells and disperse away from the source to convey inductive information through their gradient distribution (Christian, 2012; Akiyama and Gibson, 2015). It is evident that to elicit a coordinated response, cells in a receptive tissue field interpret at least three different parameters of the gradient: the signal concentration, the timing, and the direction from where they receive the signal (Briscoe and Small, 2015; Kornberg, 2016). Therefore, understanding how different cellular and molecular mechanisms in signal-producing cells prepare and release the signals at the correct time and location and at an appropriate level is fundamental to understanding tissue morphogenesis. It is also critical to know how these processes in source cells spatiotemporally coordinate and integrate with cellular mechanisms in the recipient cells to precisely shape signal gradients and tissue patterns.

To address these questions, we focused on interorgan communication of a canonical FGF family protein, Bnl, that regulates

branching morphogenesis of tracheal airway epithelial tubes in *Drosophila melanogaster* (Sutherland et al., 1996). Migration and morphogenesis of each developing tracheal branch in embryo and larvae is guided by a dynamically changing Bnl source (Sutherland et al., 1996; Jarecki et al., 1999; Sato and Kornberg, 2002; Ochoa-Espinosa and Affolter, 2012; Du et al., 2017). For instance, in third instar larva, Bnl produced by a restricted group of columnar epithelial cells in the wing imaginal disc activates its receptor Breathless (Btl) in tracheoblast cells in the transverse connective (TC), a disc-associated tracheal branch (Sato and Kornberg, 2002). Bnl signaling induces migration and remodeling of the tracheoblasts to form a new tubular branch, the Air-Sac-Primordium (ASP), an adult air-sac precursor and vertebrate lung analogue (Fig. 1 A). Such dynamic and local branch-specific signaling suggests a mechanism for precise spatiotemporal regulation of Bnl release and dispersal in coordination with the signaling response.

A critical role of regulated Bnl release can also be predicted from the way cells exchange Bnl to sculpt recipient branch-specific gradient shapes (Du et al., 2018a). Bnl is produced in the wing disc cells, but it forms a long-range concentration gradient only within the recipient ASP. Bnl gradient formation depends on signaling through actin-based signaling filopodia named cytonemes (Ramírez-Weber and Kornberg, 1999; Sato

¹Department of Cell Biology and Molecular Genetics, University of Maryland, College Park, MD; ²Cardiovascular Research Institute, University of California, San Francisco, San Francisco, CA.

Correspondence to Sougata Roy: sougata@umd.edu.

© 2019 Sohr et al. This article is distributed under the terms of an Attribution–Noncommercial–Share Alike–No Mirror Sites license for the first six months after the publication date (see <http://www.rupress.org/terms/>). After six months it is available under a Creative Commons License (Attribution–Noncommercial–Share Alike 4.0 International license, as described at <https://creativecommons.org/licenses/by-nc-sa/4.0/>).

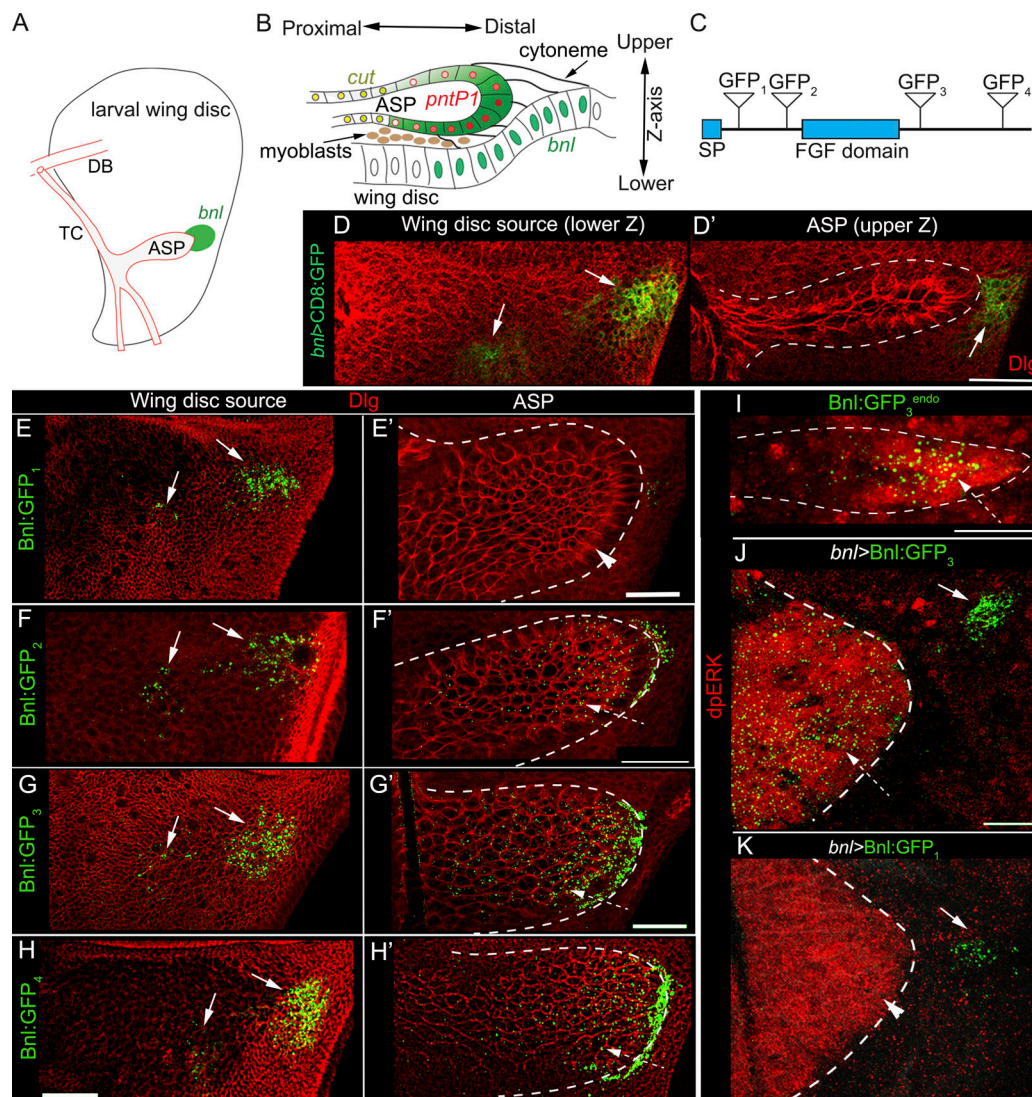


Figure 1. Separate GFP fusion sites in Bnl result in different distribution patterns. (A) Drawing depicting the organization of the ASP and *bnl*-expressing wing disc cells from third instar larva. DB, dorsal branch; TC, transverse connective. (B) Drawing of a sagittal view showing the tubular ASP epithelium, upper-lower Z-axis, ASP cytonemes that contact the disc *bnl*-source (green nuclei), and the spatial domains of *pntP1* and *cut* induced by high to low Bnl levels (green; Du et al., 2018a). (C) Schematic map of the Bnl protein backbone showing its conserved FGF domain, signal peptide (SP), and four different GFP insertion sites. (D–H') Representative images of maximum-intensity projection of lower (wing disc source) and upper (ASP) Z-sections of third instar larval wing-discs expressing CD8-GFP, Bnl-GFP₁, Bnl-GFP₂, Bnl-GFP₃, or Bnl-GFP₄ under *bnl*-Gal4 as indicated. Red, αDlg staining marking cell outlines. (I–K) Representative ASP images showing MAPK signaling (adpERK, red) zones when Bnl-GFP₃^{endo} was expressed under native cis-regulatory elements (I), and when *bnl*-Gal4 over-expressed Bnl-GFP₃ (J) or Bnl-GFP₁ (K). In D–K, white dashed line, ASP; white arrow, disc *bnl*-source; dashed arrow, Bnl-GFP puncta in the ASP; arrowhead, ASP without Bnl-GFP₁ puncta. Scale bars: 30 μm.

and Kornberg, 2002; Roy et al., 2011, 2014; Du et al., 2018a). ASP cells extend Btl-containing cytonemes to contact the basal surface of the wing disc source and directly receive Bnl (Fig. 1 B). Bnl reception through a graded number of cytonemes that are formed along the distal-proximal (D-P) axis of the ASP epithelium sculpts the Bnl gradient within the ASP. In the distal ASP cells, high to medium levels of Bnl reception through cytonemes induces an ETS transcription factor Pointed-P1 (PntP1), which elicits positive feedback on Btl synthesis and cytoneme production (Ohshiro et al., 2002; Du et al., 2018a). Gradually lower levels of Bnl reception further away from the source induce a homeobox transcription factor Cut, which suppresses Btl

synthesis and cytoneme production (Du et al., 2018a). Cut and PntP1, expressed from the opposite poles of the ASP, reciprocally antagonize each other's expression. Consequently, zones of high to low numbers of cytonemes are formed that can sculpt the Bnl gradient in coordination with recipient ASP growth. Initiation of this self-regulatory and tissue-specific gradient might require limited signal release from the source, probably only at cytoneme contact sites.

The intracellular mechanisms in the source cells that prepare Bnl for cytoneme-mediated exchange and branch-specific signaling are uncharacterized. In this study, while analyzing various functional forms of GFP-tagged Bnl, we uncovered a

posttranslational endoproteolytic modification of Bnl. We show that Bnl cleavage determines its polarized intracellular trafficking to the basal surface of the source cells from whence ASP cytonemes can receive the signal. This process limits Bnl availability to the ASP cytonemes and determines the range of Bnl gradient dispersal and tissue morphogenesis. Given the conservation of fundamental developmental signaling mechanisms, our demonstration of how a signal is endowed with information for its target-specific intercellular distribution has fundamental implications for understanding tissue morphogenesis.

Results

Bnl:GFP chimeras with different tag sites show different dispersion patterns

To identify various functional forms of GFP-tagged Bnl proteins, we generated four different Bnl:GFP variants and examined their signaling activities (Fig. 1, A–C; Materials and methods; and Tables S1 and S2). The Bnl protein is 770 amino acids long, with an N-terminal 31-residue signal peptide and a conserved FGF domain spanning from amino acids 243 to 379 (Fig. 1 C). Each of the four variants contained a GFP tag at a single internal site: at the 87th (Bnl:GFP₁), 206th (Bnl:GFP₂), 432nd (Bnl:GFP₃), and 701st (Bnl:GFP₄) amino acid residue. Transgenic *Drosophila* lines harboring these constructs were crossed to *bnl-Gal4* flies and analyzed for activity in third instar larvae. In 3D confocal stacks of wing discs, the lower Z sections revealed the Bnl-expressing cells in the wing disc columnar epithelium, and the upper Z sections (close to the objective) showed the associated ASP (Fig. 1, B, D, and D'; and Video 1).

When the Bnl:GFP variants were expressed under *bnl-Gal4* control, all of the variants were detected in the disc Bnl source as bright fluorescent puncta (Fig. 1, E–H). Overexpression of all four Bnl:GFP variants led to ASP overgrowth (Fig. 1, E–H'), which phenocopied a Bnl overexpression condition (Sato and Kornberg, 2002). Thus, all of the Bnl:GFP variants could signal nonautonomously. Unlike a membrane-tethered CD8:GFP protein, the fluorescent puncta comprising Bnl:GFP₂, Bnl:GFP₃, and Bnl:GFP₄ were detected in the recipient ASP, suggesting that the signals moved from the source to the ASP (Fig. 1, D–H'; and Video 2). Surprisingly, although Bnl:GFP₁ puncta were visible in the source cells and its overexpression induced ASP overgrowth, the fluorescent puncta were absent from the recipient ASP (Fig. 1, E–E'; Fig. S1, A–B'; and Video 3). Generally, as shown with an ASP derived from a genome-edited *bnl:GFP₃^{endo}* larva that expressed the Bnl:GFP₃ at physiological levels (Du et al., 2018a), only the distal ASP cells with high to moderate levels of Bnl induce MAPK signaling (Fig. 1 I). In contrast, overexpression of Bnl:GFP₃ or Bnl:GFP₁ in the source activated MAPK signaling in all of the ASP cells (Fig. 1, J and K). Thus, Bnl:GFP₁, like Bnl:GFP₃, is an active signal, but GFP fluorescence was undetectable in the recipient ASP.

Bnl is cleaved before its transport to the recipient ASP

One possibility for Bnl:GFP₁ being functional yet undetectable in the ASP could be that the protein was cleaved downstream of tagging site 1 before the interorgan transport of its untagged

C-terminal fragment (Fig. 1 C). To test this possibility, we generated a double-tagged Bnl chimera with HA inserted at site 1 and GFP inserted at site 3 (Fig. 2 A). We performed Western blot analyses on total protein lysates of cultured S2 cells that were transfected with the *bnl:GFP₁*, *bnl:GFP₃*, or *bnl:HA₁GFP₃* constructs. An α GFP antibody recognized a common 150-kD band, which likely represented the full-length protein (Fig. 2 B). Although the molecular weight of full-length Bnl:GFP was predicted to be ~113 kD, a larger band size could be due to posttranslational modifications. Similar observations were reported earlier for two *Drosophila* FGFs, Pyramus and Thisbe (Tulin and Stathopoulos, 2010). Bnl:HA₁GFP₃ and Bnl:GFP₃ had similar band profiles, but Bnl:GFP₁ and Bnl:GFP₃ had multiple variant-specific bands (Fig. 2 B). The detection of unique smaller bands (~37 and 60 kD) for N-terminally tagged Bnl:GFP₁ and unique larger bands (>100 kD) for C-terminally tagged Bnl:GFP₃ or Bnl:HA₁GFP₃ was consistent with a cleavage near tagging site 1. An α HA antibody recognized a weak ~20-kD band (Fig. S2, A and B) from lysates containing Bnl:HA₁GFP₃ and Bnl:HA₁ (HA-tag at position 1), but not from Bnl:HA₃ (HA-tag at site 3). Therefore, the ~20-kD band represented the N-terminal cleaved product. These biochemical analyses suggested a cleavage in the Bnl backbone, but it was difficult to estimate the actual molecular size of the cleaved bands. Furthermore, the intracellular and intercellular fates of the cleaved products cannot be directly visualized in tissues using biochemical assays.

Therefore, we used a fluorescence microscopy-based assay to simultaneously visualize both the HA- and GFP-tagged parts of Bnl in cells. Immunostaining with α HA in S2 cells harboring uncleaved Bnl:HA₁GFP₃ molecules was expected to show both HA₁ and GFP₃ localizing together. In contrast, a cleavage in the molecules would separate the HA₁ tag from GFP₃. Indeed, in transfected S2 cells, Bnl:HA₁GFP₃ was present in two distinct spatially separated forms (Fig. 2, C–F). An internal perinuclear zone showed colocalized GFP and HA signal, suggesting that the zone contained uncleaved Bnl. In addition, there were a number of exclusively GFP-positive puncta that localized more toward the periphery of the S2 cells. Cells that were cultured and allowed to adhere to a coverslip contained peripheral lamellipodial and filopodial projections at the adherent surface. These peripheral lamellipodial/filopodial projections contained only a truncated Bnl:GFP portion (Fig. 2, D–F; and Videos 4 and 5). Spatial separation of the C-terminal GFP-tagged portion from the rest of the Bnl:HA₁GFP₃ molecule suggested Bnl cleavage.

To further test the peripheral distribution of the truncated C-terminal fragment, we generated two different constructs: *bnl:HA₁GFP₄* and *bnl:GFP₁HA₄*, where the HA and GFP tags were interchanged between sites 1 and 4 (Materials and methods). Although the tag positions were changed in these constructs, irrespective of the tags and tagging sites the cleaved N- and C-terminal Bnl fragments showed consistent subcellular localization patterns (Fig. S2, C and D). These results showed that Bnl is cleaved and a truncated C-terminal portion is trafficked toward the cell periphery, probably for release. To test interorgan dispersion of cleaved/uncleaved forms of Bnl, we generated transgenic *Drosophila* lines harboring the *bnl:HA₁GFP₃* construct. When *bnl-Gal4* overexpressed Bnl:HA₁GFP₃

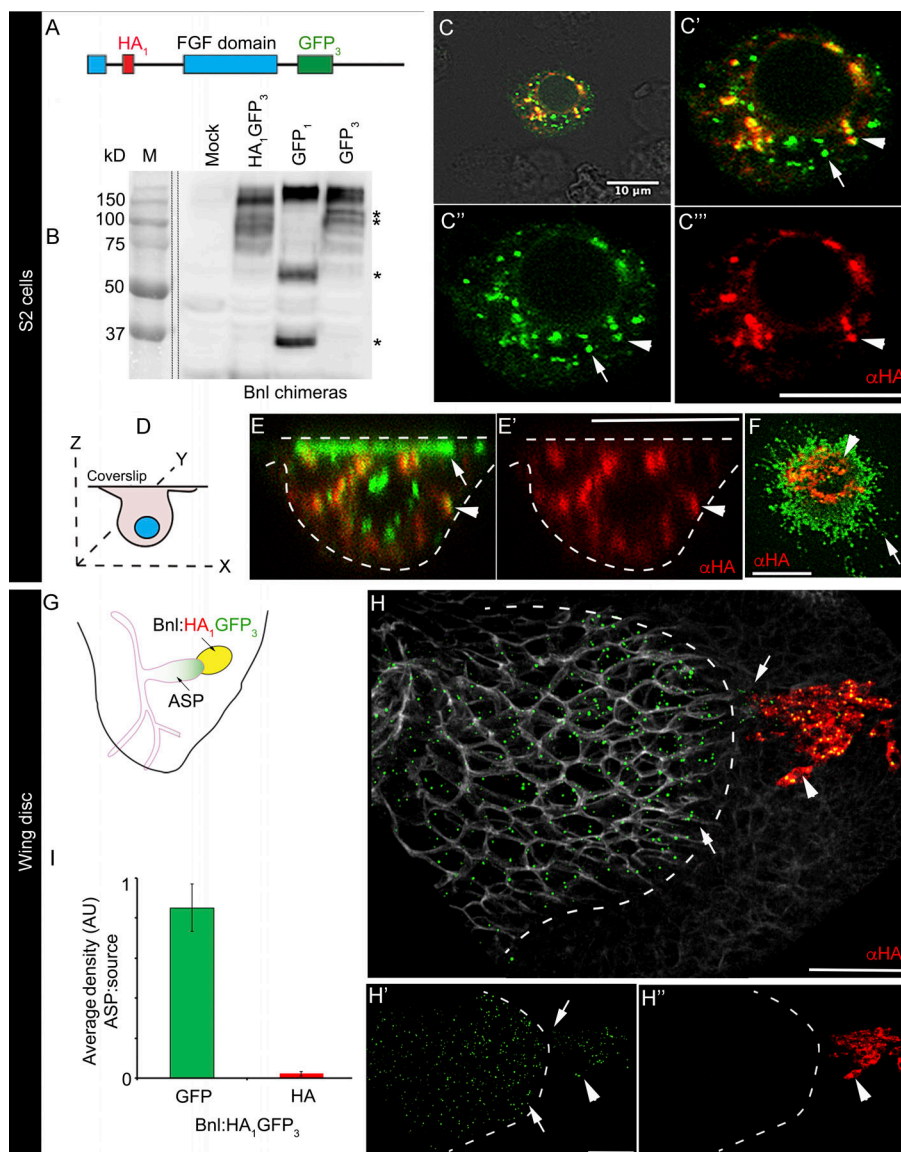


Figure 2. Bnl is cleaved in producing cells before its transport to the recipient ASP. (A) Schematic map of a dual-tagged Bnl:HA₁GFP₃ construct containing an HA-tag at site 1 and a GFP-tag at site 3. **(B)** An αGFP Western blot showing differential bands (*) obtained from S2 cell lysates containing Bnl:HA₁GFP₃, Bnl:GFP₁, and Bnl:GFP₃. Mock, lysates from untransfected cells. **(C–F)** Representative images of αHA-immunostained (red) S2 cells expressing Bnl:HA₁GFP₃; examples from adherent cells grown on coverslip (D–F): XYZ section (E and E') and XYZ section near coverslip (F); merged bright field and fluorescent (C), merged fluorescent (C', E, and F), and split channels shown (C'', C''', and E'). **(G)** A schematic drawing showing the expected localization pattern of the uncleaved Bnl:HA₁GFP₃ (yellow) and truncated Bnl:GFP₃ derivative (green) in the αHA-stained (red) discs/ASP. **(H and I)** A representative image of an αHA-stained (red) wing disc and ASP (dashed line) when *bnl-Gal4* expressed Bnl:HA₁GFP₃ (*UAS-bnl:HA₁GFP₃*). White, αDlg; split channels (H' and H''); a graph (I) comparing the fractions of GFP and HA (αHA) signal in the recipient ASP relative to that of the wing disc source (*n* = 14) under this condition. In C–H'', arrowhead, uncleaved Bnl:HA₁GFP₃; arrow, truncated Bnl:GFP₃ derivative of Bnl:HA₁GFP₃. Scale bars: 10 μm (C–F); 30 μm (H–H'').

in the wing disc source, the N-terminal HA-tagged portion of Bnl remained in the signal-producing cells, and a truncated GFP-tagged C-terminal portion of Bnl (Bnl:GFP₃) localized only in the recipient ASP cells (Fig. 2, G–I; and Fig. S2, E–G''). These results strongly suggested that Bnl is cleaved in the source and only a truncated Bnl derivative is received by the ASP.

Bnl is cleaved at a single endoproteolytic site in the Golgi network

Evolutionarily conserved serine proteases, namely the proprotein convertases (PCs) that include Furins, cleave many growth factors and hormones that are synthesized in the form of proligands (Thomas, 2002). With an artificial neural network-based in silico PC site prediction tool (Duckert et al., 2004), we identified three putative PC sites (PCS1–3) in the Bnl backbone. Among them, PCS1 was Furin-specific with a core R-X-[R/K]-R domain (Fig. 3, A–A'). Coincidentally, the four selected tagging sites in the Bnl backbone were perfectly structured for testing

the putative cleavage sites (Fig. 3 A). To test for cleavage at PCS3 (Fig. 3 A), we generated a chimeric Bnl:GFP₃HA₄ construct in which the GFP and HA tags were inserted at sites 3 and 4, respectively. Immunostaining with an αHA antibody on S2 cells transfected with *bnl:GFP₃HA₄* showed colocalization of GFP₃ and HA₄ (Fig. 3 B). Based on this cell biological assay, PCS3 is an unlikely cleavage site. However, we did not investigate the possibility of potential PCS3 cleaved products remaining closely associated during their intracellular trafficking. In contrast, a cleavage at either PCS1 or PCS2 could explain the observed differential distribution of the N and C portions of Bnl:HA₁GFP₃ (Fig. 2, C–H).

To test PCS1 and PCS2, we replaced their arginine (R) residues with glycine (G) and generated *bnl:HA₁GFP₃-M1* (henceforth referred as M1), a construct with mutations in PCS1 ((R/G)₁₆₁TE (R/G)₁₆₄^SI(R/G)₁₆₆), and *bnl:HA₁GFP₃-M2* (henceforth referred as M2) with mutations in PCS2 ((R/G)₂₃₃NE(R/G)₂₃₆^; Fig. 3 A). R-to-G substitutions in PC sites were shown to successfully block PC cleavage (Künnapuu et al., 2009). In transfected S2 cells,

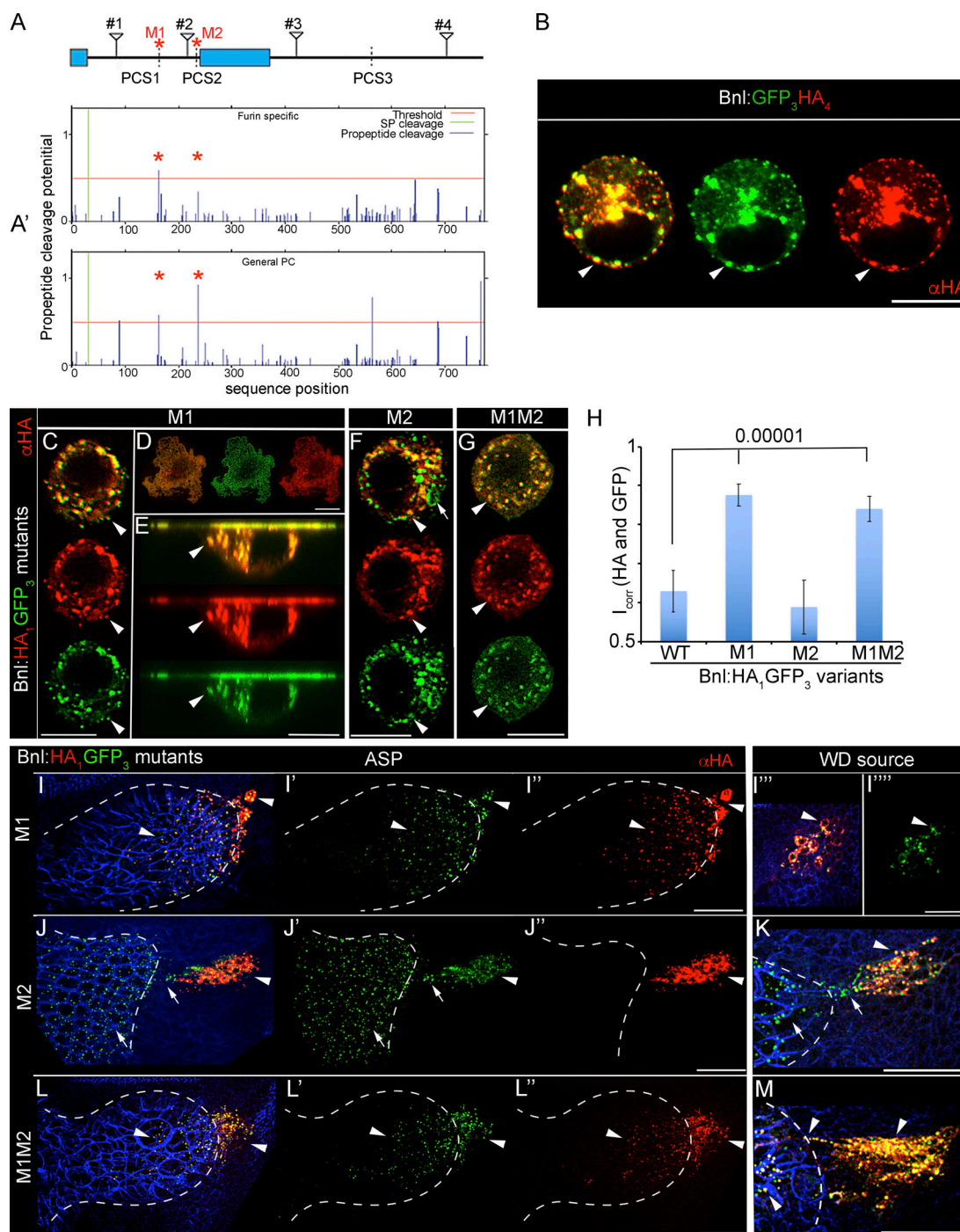


Figure 3. Bnl is cleaved at a single endoproteolytic site. (A) Location of putative PCS1-3 in the Bnl backbone. #1-4: GFP insertion sites; *, point mutations generated at PCS1 (M1) and PCS2 (M2). (A') In silico predictions of PC sites. Upper panel, Furin-specific; lower panel, for general PC; green line, SP cleavage site; red line, a set threshold above which the sequence is predicted to be a PC site. (B-G) Examples of αHA immunostained (red) S2 cells expressing Bnl:GFP₃HA₄ (B) and Bnl:HA₁GFP₃ mutants as indicated (C-G); XYZ section near coverslip (D) and XYZ section (E) of M1-expressing adherent cells. (H) Graphs comparing colocalization index (I_{corr}) of the HA- and GFP-tagged parts of Bnl:HA₁GFP₃ (WT), M1, M2, and M1M2 in αHA-stained (red) S2 cells. $n = 15$ (WT), 13 (M1), and 9 (M2 and M1M2); P values: ANOVA followed by Tukey HSD. In B-G, S2 cells were cotransfected with *act-Gal4* and *UAS-X*, X = constructs as indicated. (I-M) Maximum-intensity projections of the wing-disc source (I', I'', I''', K, and M) expressing Bnl:HA₁GFP₃ mutants as indicated (*bnl-Gal4* x *UAS-X*, X = M1, M2, M1M2) and the recipient ASPs (I-I'', J-J'', and L-L''). Blue, αDlg; white dashed line, ASP. In B-M, arrow, truncated Bnl:GFP₃ derivative; arrowhead, uncleaved Bnl:HA₁GFP₃. Scale bars: 10 μm (B-G); 30 μm (I-M).

PCS1 mutation rendered the M1 molecules uncleavable, as HA and GFP colocalized in the intracellular compartments (Fig. 3, C-E; and Video 6). However, M2 molecules were cleaved like WT

proteins (Fig. 3 F). To compare the cleavage efficiency among the Bnl mutants, we estimated the fraction (index of correlation [I_{corr}]) of colocalized pixels of HA and GFP channels from 3D

images (Jaskolski et al., 2005). The average I_{corr} value was significantly higher for M1 and M1M2 than either the control Bnl:HA₁GFP₃ or M2 cells, suggesting that the PCS1 mutation inhibited cleavage (Fig. 3 H). We also generated transgenic flies harboring the M1, M2, or M1M2 constructs and analyzed their distribution in the disc and ASP. When the M1 and M1M2 mutants were expressed in the wing disc source, the recipient ASPs received the colocalized HA-GFP puncta comprising the uncleaved full-length molecules (Fig. 3, I-I''' and L-M; and Video 7). In contrast, only the GFP-tagged C-terminal part of M2 was distributed within the ASP (Fig. 3, J and K). Collectively, these results suggest that Bnl:HA₁GFP₃ molecules are cleaved at PCS1 before their delivery from the disc source to the ASP.

Bnl cleavage could be intracellular or, alternatively, could occur on the surface of the source cell plasma membrane where the signal is delivered to the recipient ASP cytonemes (Fig. 1 B). To test this possibility, we employed a detergent-free αGFP-based immunostaining protocol (henceforth referred to as αGFP^{ex}), which was previously used to detect surface-exposed Bnl:GFP (Du et al., 2018a). The αGFP^{ex} assay detected only Bnl:GFP₃ on the expressing source cell surface, but not Bnl:GFP₁ (Fig. 4, A and B). Thus, Bnl cleavage is intracellular, and only the truncated C-terminal Bnl portion is displayed on the basal surface of the source cells. To determine the subcellular location of Bnl cleavage, we performed standard immunostaining with αGM130 antibody, a cis-Golgi probe, on discs expressing Bnl:GFP₁, Bnl:HA₁GFP₃, or Bnl:HA₁GFP₃-M1. In the wing disc source, 100% of either Bnl:GFP₁ or uncleaved Bnl:HA₁GFP₃ puncta were localized in the GM130-marked cis-Golgi (Fig. 4, C-D'), whereas the truncated Bnl:GFP₃ derivative (GFP-only puncta) localized in many small uncharacterized intracellular vesicles, some of which were enriched with Syntaxin16, a target-SNAP receptor for intra/trans-Golgi sorting (Charnig et al., 2014; Fig. 4, D, D', F, and F'). On the other hand, uncleaved M1 puncta were seen in all of the vesicular compartments, indicating their routing through the secretory pathway (Fig. 4, E, E', G, and G'). Similar intracellular distribution profiles of the cleaved and uncleaved portions of Bnl were observed in cultured S2 cells (Fig. 4, H-J'). Collectively, these results showed that Bnl is cleaved during its trafficking through the Golgi network.

Bnl is cleaved by Furin1 in the wing disc *bnl* source

Intracellular Bnl cleavage at PCS1, which is a Furin-specific site, indicated that Bnl is likely cleaved by a Furin. To identify the specific protease, we performed RNAi-mediated knockdown of two *Drosophila* furin genes, *Dfurin1* (*fur1*) and *Dfurin2* (*fur2*), in cell culture assay. We did not investigate the role of *amontillado* (*amon*), a mammalian PC2 orthologue, since it is expressed only in neurons and neuroendocrine cells (Roebroek et al., 1992, 1993; Künnapuu et al., 2009). In S2 cells, RNAi treatment of *fur1*, *fur2*, or both significantly reduced Bnl:HA₁GFP₃ cleavage in comparison to a nonspecific control RNAi (Fig. 5, A-E). Thus, Bnl cleavage is Fur1 and Fur2 dependent. However, in vivo, only *fur1* knockdown in the wing disc *bnl* source resulted in a stunted ASP development, which phenocopied the *bnl* knockdown condition (Fig. 5, F-I; Fig. S3, A-D; and Table S3). Measurement of the allometric ratio of the recipient ASP length along its major D-P

axis to the width of the wing disc confirmed that the growth abnormality was ASP specific and was not due to a systemic developmental delay (Fig. 5, J and J'). Lack of a *fur2* knockdown phenotype in the ASP is likely due to the absence of *fur2* expression in the *bnl* source, as expression analyses of *fur1* and *fur2* showed only *fur1* expression in the *bnl* source (Fig. S3, E-K). Thus, although both Fur1 and Fur2 could cleave Bnl in S2 cells, their substrate specificity might depend on their tissue-specific expression.

The RNAi analyses provided correlative evidence of Furin's role in Bnl cleavage. For direct evidence, we ex vivo cultured larval wing discs expressing Bnl:HA₁GFP₃ in the *bnl* source in either the presence or absence of Furin inhibitors. In spite of the prolonged (up to 16 h) ex vivo culture conditions, Bnl:HA₁GFP₃ was cleaved in the absence of inhibitors, and the truncated Bnl:GFP₃ moved to the growing ASPs (Fig. 6, A-C'). In the presence of inhibitors (Fig. 6, D-F'), Bnl cleavage in the disc source was blocked, and the amount of uncleaved puncta received by the ASP gradually increased with the increase in incubation time (Fig. 6 G). The time-dependent inhibition of Bnl cleavage by Furin inhibitors confirmed Furin-dependent Bnl cleavage. Importantly, these results, together with the M1 mutant analyses (Fig. 2 I), showed that when Bnl cleavage is blocked the uncleaved signals can still move from the disc to the ASP. These results indicated that cleavage might not be essential for molecular activation of the Bnl protein and led us to examine the physiological roles of Bnl cleavage.

Uncleaved Bnl can signal and is dispersed by cytonemes, but only within a narrow range

To examine M1 distribution and activity at its physiological levels of expression, we modified a previously reported *bnl*:GFP₃^{endo} allele into *bnl*:HA₁GFP₃^{endo} (henceforth referred as *wt*^{endo}) and corresponding *bnl*:HA₁GFP₃-M1^{endo} mutant alleles (henceforth referred as *m1*^{endo}) by using genome editing (Materials and methods; Fig. 7 A). Consistent with earlier observations for *bnl*:GFP₃^{endo} (Du et al., 2018a), *wt*^{endo} flies were homozygous viable and had normal tissue morphology (Table S4). Although *bnl* is an essential gene, *m1*^{endo} mutant flies were homozygous viable, indicating that the PCS1 mutation was nonlethal. As expected, the endogenous Bnl:HA₁GFP₃^{endo} (WT^{endo}) molecules were cleaved and ASPs received only the truncated Bnl:GFP₃ portion (henceforth referred as t-WT^{endo}; Figs. 7 B and S4 A). The *m1*^{endo} ASPs also received uncleaved Bnl:HA₁GFP₃-M1^{endo} (henceforth referred as M1^{endo}) puncta containing both HA and GFP (Figs. 7 C and S4 B). Furthermore, ex vivo cultured *wt*^{endo} wing discs grown in the presence of Furin inhibitors had uncleaved Bnl:HA₁GFP₃^{endo} puncta in the ASP (Fig. 7, D and E). Thus, in the absence of cleavage, uncleaved Bnl could move to the ASP and sustain tracheal growth.

When we genetically combined either *wt*^{endo} or *m1*^{endo} with a *btl*:cherry^{endo} allele, which expressed endo-tagged Btl:Cherry (Du et al., 2018a), both t-WT^{endo} and M1^{endo} puncta colocalized with the receptors in the ASPs (Fig. 7, F-G'). As reported earlier (Du et al., 2018a), the distal ASP tip, which is closest to the disc *bnl* source, had a high concentration of the receptor-colocalized t-WT^{endo} or M1^{endo} puncta. With increasing distance from the

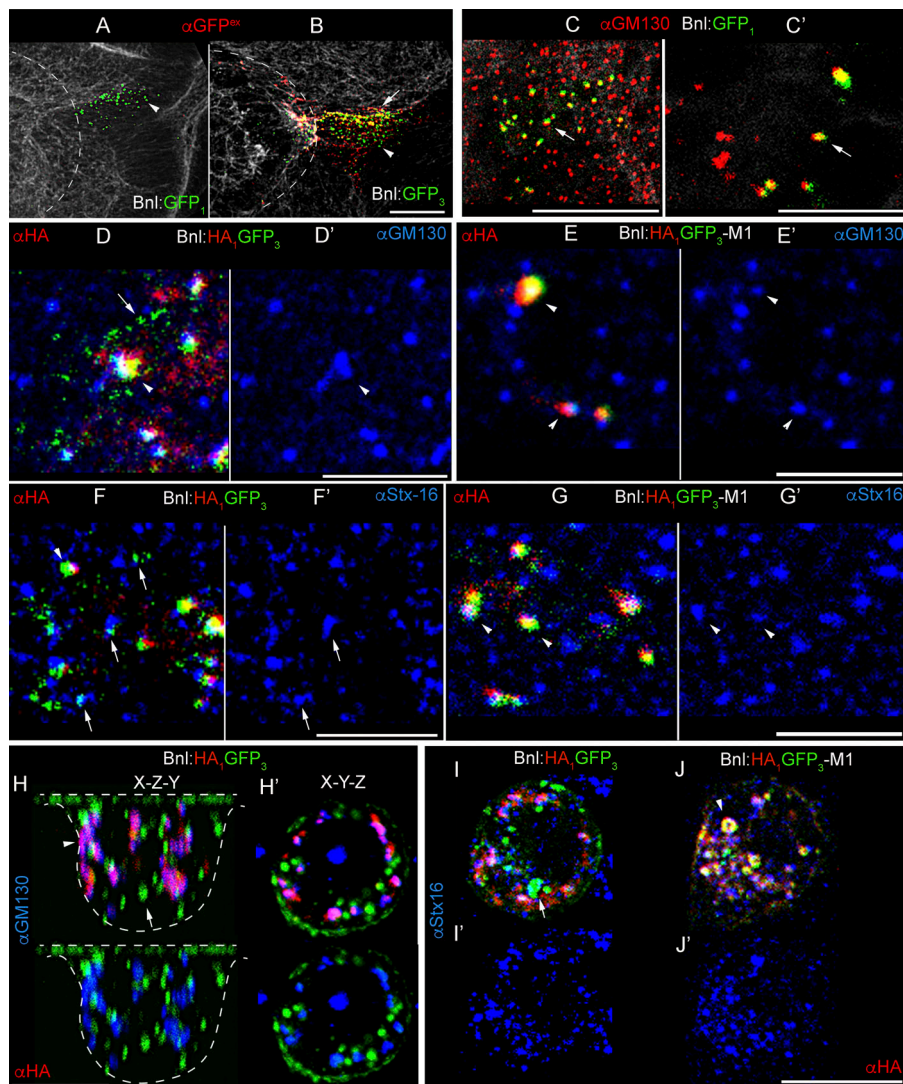


Figure 4. Bnl is cleaved in the Golgi network of Bnl-producing cells. (A and B) Projection images of lower Z-stacks of the disc *bnl* source showing detergent-free α GFP immunostaining (α GFP^{ex}, red) when *bnl-Gal4* expressed Bnl:GFP₁ (A) and Bnl:GFP₃ (B). White, phalloidin-Alexa Fluor 647 to mark actin-rich cell outlines; arrowhead, intracellular Bnl:GFP (only green); arrow, surface-localized Bnl:GFP (green+red); dashed line, ASP in the upper Z-stacks (not shown). **(C and C')** α GM130-stained (red) optical sections of wing disc *bnl*-source expressing Bnl:GFP₁. **(D-J')** Single optical sections of α HA-immunostained (red) disc *bnl*-source (D-G') and S2 cells (H-J') expressing either Bnl:HA₁GFP₃ or M1 and marked with α -Stx-16 or α GM130 (blue) as indicated. Arrow, truncated Bnl:GFP₃ derivative; arrowhead, uncleaved Bnl:HA₁GFP₃ or M1 mutant; merged (D-J) and split (D'-J') blue channels shown. Scale bars: 20 μ m (A-C); 5 μ m (C'-G'); 10 μ m (H-J').

source, their concentration gradually decreased. Bnl is known to be transported by cytonemes to form a receptor-associated gradient (Du et al., 2018a). To examine cytoneme-mediated transport, we live imaged CD8:Cherry-marked ASPs in the homozygous *wt*^{endo} or *ml*^{endo} larvae (>30 discs/genotype). In both conditions, ASPs extended long (>15- μ m) polarized cytonemes toward the source cells and received GFP-tagged fluorescent puncta comprising either t-WT^{endo} or M1^{endo} (Fig. 7, H-I'; and Fig. S4, C and D). Surface α GFP^{ex} immunostaining showed that both M1^{endo} and t-WT^{endo} colocalized with Btl:Cherry^{endo} on the recipient cytoneme surfaces before their endocytosis (Fig. 7, J and J'; and Fig. S4, E-F'). Therefore, the pattern of tissue-specific dispersion of M1^{endo} was comparable to that of t-WT^{endo}.

However, thorough scrutiny revealed that the *ml*^{endo} allele produced hypermorphic phenotypes due to a reduced signaling range. The distal tip area of *ml*^{endo} ASPs had significantly fewer long (>15- μ m) signal-receiving cytonemes than the *wt*^{endo} ASPs (Fig. 7 K). All of the cells (~6-7 cells in Z-projected images) within a 60- μ m periphery surrounding the tip of *wt*^{endo} ASPs extended long signaling cytonemes. In contrast, only one to two distal tip cells in the comparable region of the *ml*^{endo} ASPs

extended M1^{endo}-receiving cytonemes. A restricted zone of M1^{endo}-receiving cytonemes is reflected in the narrow gradient range and attenuated *ml*^{endo} ASP growth (Fig. 8, A-E). While t-WT^{endo} formed a long-range gradient along the ~10-12-cell-long ASP D-P axis, M1^{endo} formed a narrow, steeper gradient along the ~5-6-cell-long D-P axis (Fig. 8, D and E). Accordingly, the *ml*^{endo} ASPs had a reduced zone of nuclear dpERK in comparison to the *wt*^{endo} ASPs (Fig. 8, G-I). Thus, M1^{endo} had a narrow distribution and signaling range compared with t-WT^{endo} (Fig. 8, G-I; and Fig. S4, G and H). Nevertheless, normalization of either the signal concentration or the signaling zone with recipient ASP length showed comparable scaling of the t-WT^{endo} and M1^{endo} gradients and signaling zones in relation to the recipient ASP size (Fig. 8, F and I). Previously, our work suggested that the Bnl gradient adopts recipient ASP-specific shapes due to two counteracting Bnl signaling feedbacks on cytonemes (Du et al., 2018a). Thus, scaling of the M1^{endo} gradient to the recipient-specific shape indicated normal M1^{endo} signaling, but within a limited range.

Ectopic expression in the salivary gland, a nontracheated organ that does not normally express *bnl* (Jarecki et al., 1999),

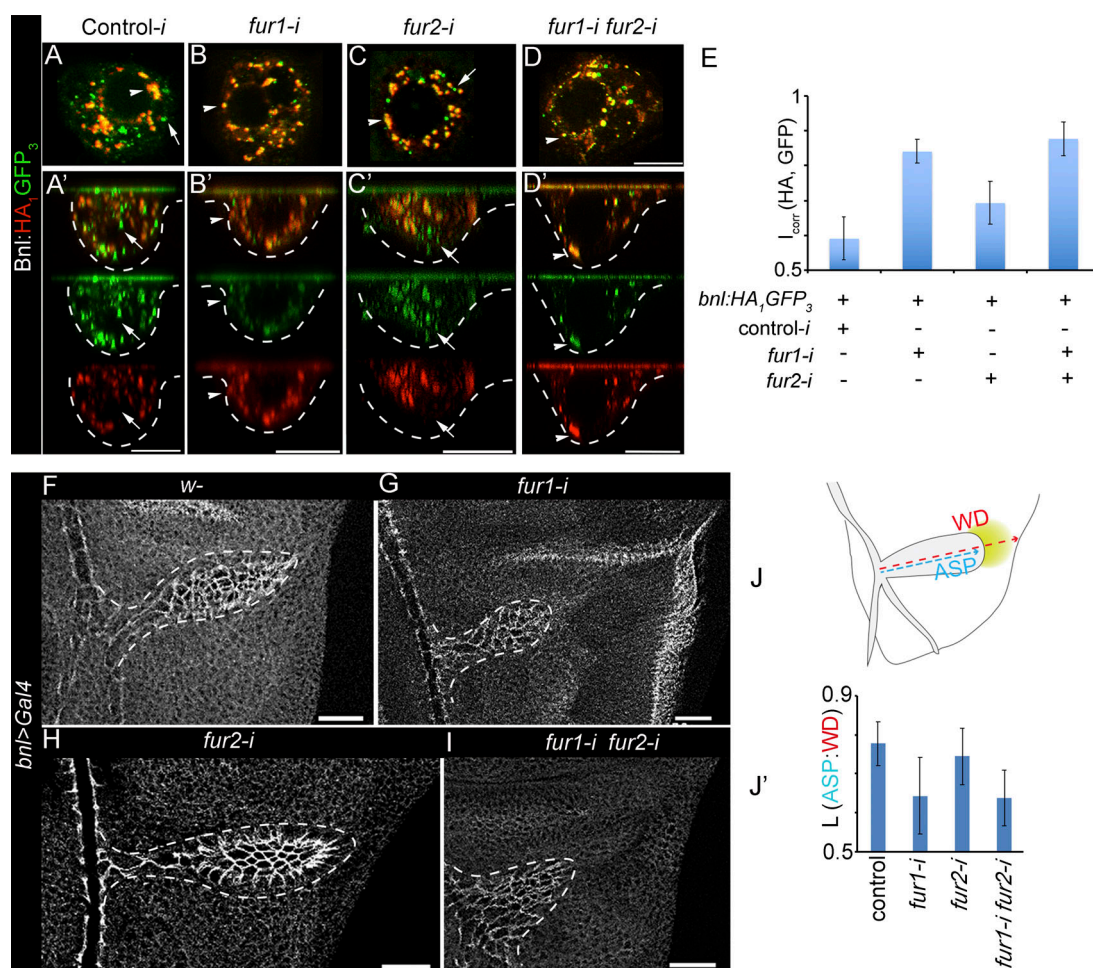


Figure 5. Knockdown of *furin* expression affects Bnl cleavage. (A–D') Images of α HA-immunostained (red) S2 cells cotransfected with *act-Gal4*, *UAS-bnl:HA₁GFP₃*, and the synthesized RNAi as indicated. Control-*i*, nonspecific dsRNA; XYZ (A–D) and XZY (A'–D') views; arrow, truncated Bnl:GFP₃ derivative; arrowhead, uncleaved Bnl:HA₁GFP₃. (E) Graph comparing Bnl:HA₁GFP₃ cleavage under various *furin* knockdown conditions in S2 cells. I_{corr} index of HA and GFP colocalization, with lower values indicating cleavage and color separation; $n = 13$ (control), 11 (*fur1-i*), 12 (*fur2-i*), and 14 (*fur1-i fur2-i*); P values (ANOVA followed by Tukey HSD): *fur1-i* versus *fur1-i fur2-i*, $P = 0.347$; all other groups, $P < 0.001$. (F–I) α Dlg-immunostained (white) wing disc and ASP (white dashed line) from larvae where *bnl-Gal4* expressed *furin* RNAi as indicated. Control, *bnl-Gal4* \times *w⁻*. (J and J') Drawing depicting the scheme (J) of allometric measurement of ASP length (L) relative to the corresponding wing disc (WD); graph (J') comparing the length (L) ratio of ASP to wing-disc (WD) under conditions indicated. $n = 48$ (control), 95 (*fur1-i*), 86 (*fur2-i*), 102 (*fur1-i fur2-i*); P values (ANOVA followed by Tukey HSD): all groups versus *fur1-i*, $P < 0.001$; all groups versus *fur1-i fur2-i*, $P < 0.001$. Scale bars: 10 μ m (A–D); 30 μ m (F–I).

also showed a limited spatial distribution and signaling of M1. Since Bnl expression is known to induce tracheal invasion toward source cells, active Bnl expression in the salivary gland was expected to induce easily scorable tracheal invasion. We took advantage of a nonspecific expression of *bnl-Gal4* (Du et al., 2017) in the salivary gland to express the Bnl mutants. Except for a CD8:GFP control, equivalent levels of expression of Bnl:HA₁GFP₃ (WT), M1, M2, or M1M2 all induced tracheal invasion into the salivary gland, confirming their nonautonomous signaling irrespective of cleavage (Fig. 8, J–N; and Fig. S5 A). Thus, M1 is an active signal. However, the salivary glands expressing WT and M2 had a significantly higher number of terminal branches ramifying throughout the gland surface. In contrast, glands expressing M1 or M1M2 showed poor terminal branching frequencies and surface coverage (Fig. 8, K–O). Thus, M1 induced a spatially restricted response on the source cell surface. Since Bnl

distribution pattern on a producing cell surface determines the spatial coverage of terminal branching on it (Peterson and Krasnow, 2015), attenuated terminal branching on the M1-expressing salivary glands suggested a reduced availability of M1 on the exposed basal cell surface of the salivary gland.

Bnl cleavage ensures its trafficking to the basal cell surface

To examine this possibility, we performed the surface α GFP^{ex} assay on salivary glands expressing the M1 or WT constructs. As expected, a significantly lower fraction of total M1 molecules were externalized on the basal surface of the salivary gland cells in comparison to WT (Fig. 9, A–D). Strikingly, while the WT protein covered the entire basal surface of the giant-sized salivary gland cells, most of the externalized M1 molecules were restricted to the cell junctions (Fig. 9, B and B'). Such abnormality in spatial distribution might suggest mispolarized M1

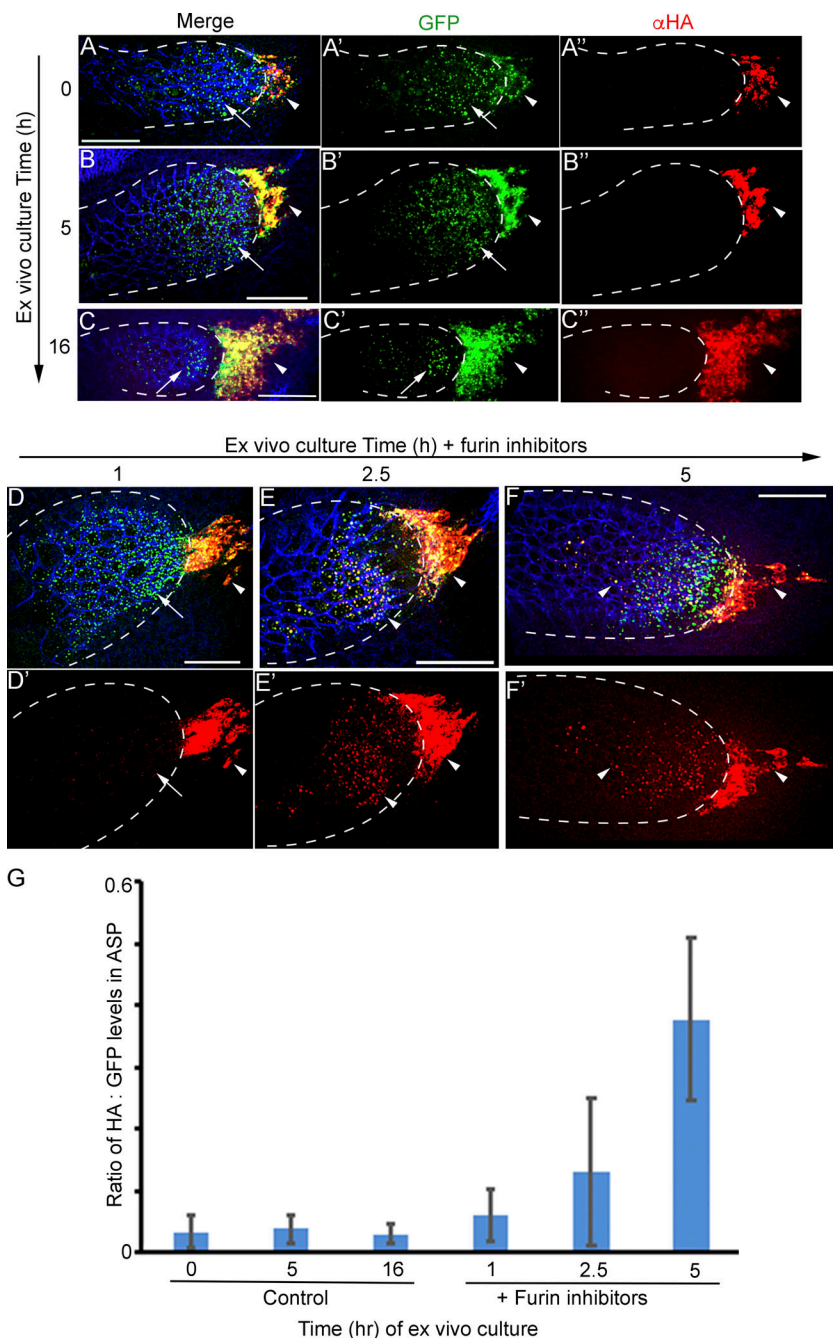


Figure 6. Furin-dependent Bnl cleavage in the wing disc. (A–F') The α HA-stained (red) wing disc that expressed Bnl:HA₁GFP₃ under *bnl-Gal4* and were ex vivo cultured for 0 (pretreat) to 16 h in the absence and 1–5 h in the presence of Furin inhibitors as indicated. Arrow, truncated Bnl:GFP₃ derivative; arrowhead, uncleaved Bnl:HA₁GFP₃; blue, phalloidin-Alexa Fluor 647 marking cell outlines; merged (A–D) and either split green, red (A'–C'') or only red (D'–F') channels are shown. **(G)** Graphs comparing average levels of colocalized HA and GFP in the ASP grown in presence and absence of Furin inhibitors; samples were harvested at different time points from the continuous culture. $n = 11$ (0 h), 11 (1 h), 10 (2.5 h), 9 (5 h control), 12 (5 h test), 5 (16 h); P values (ANOVA followed by Tukey HSD): $P = 0.0001$ for 5 h versus either 0 h, 1 h, or 2.5 h of Furin inhibition. Scale bars: 30 μ m.

trafficking, reducing its availability at the basal surface. Indeed, confocal sections through the salivary glands showed that most M1 signals were selectively enriched at the apical luminal sides of the cells that were inaccessible to the external trachea (Fig. 9, E–H). Notably, although salivary gland cells do not express Bnl, they contain the Bnl cleavage machinery. Bnl:HA₁GFP₃ (WT) driven by *bnl-Gal4* was cleaved leading to clear spatial separation of the HA- and GFP-tagged fragments (Fig. S5, B and B'). Therefore, these results suggested that Bnl cleavage promotes efficient polarized trafficking to the basal signaling surface from whence tracheal cells can receive the signal.

To confirm polarized Bnl sorting in the wing disc source, we acquired XZY sections of the disc-ASP tissue complex along the

ASP D–P axis (Fig. 9, I–M). In the CD8:Cherry-marked disc *bnl* source, overexpressed M1 molecules preferentially populated the apical luminal and lateral sides of the columnar epithelial cells. In contrast, the truncated WT molecules had relatively higher density toward the basal side of the source cells (Fig. 9, J–L). In α HA-immunostained discs that expressed the Bnl:HA₁GFP₃ construct under *bnl-Gal4*, the truncated Bnl:GFP₃ signal was clearly polarized toward the basal surface of the columnar epithelial cells facing the overlying ASP (Fig. 9 M). A surface α GFP^{ex} assay confirmed a higher percentage of basal externalization of Bnl:GFP₃ compared with M1 (Fig. S5 C). Similarly, when examining the genome-edited *wt^{endo}* and *ml^{endo}* larvae, we found that the basal surface of the disc source and recipient ASP

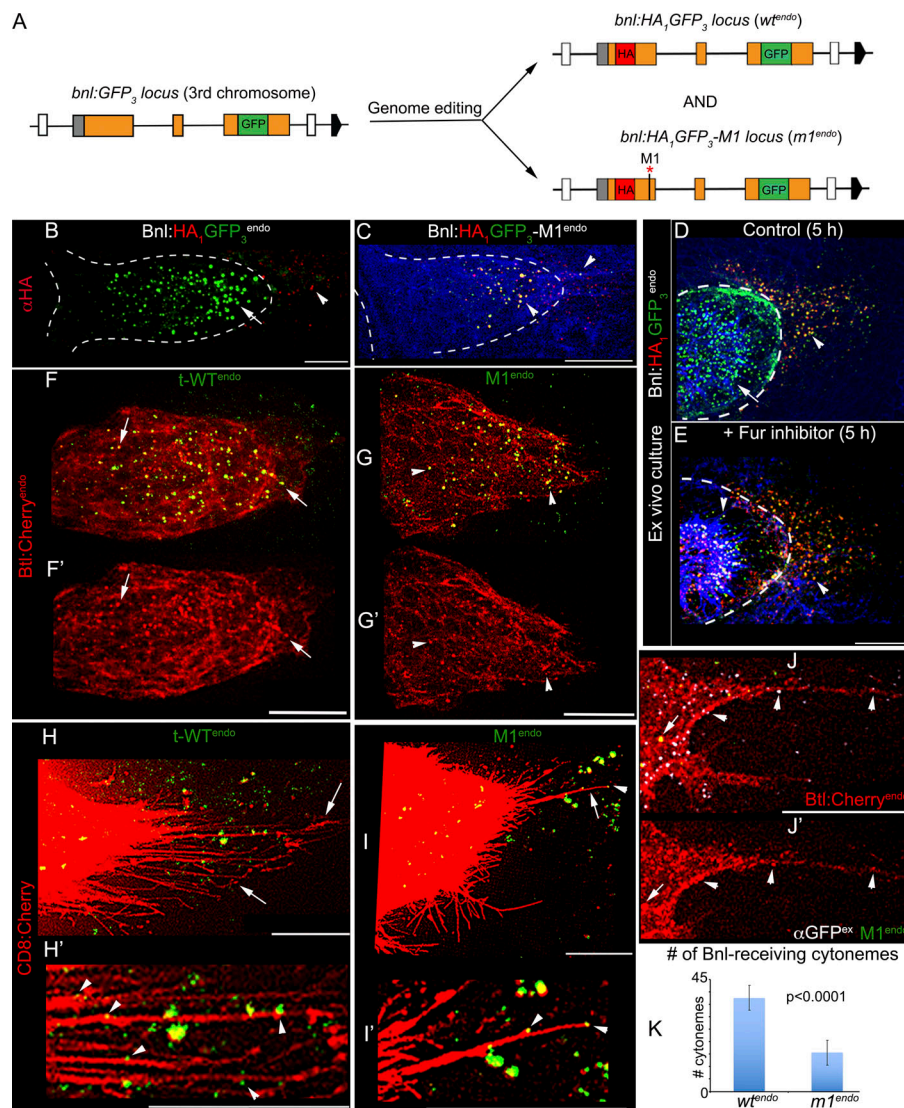


Figure 7. Comparison of activities of endogenously expressed cleaved and uncleaved Bnl. (A) Schematic map of the genomic *bnl:GFP₃* locus and the products of its subsequent CRISPR/Cas9-based editing; orange box, coding exon; gray box, noncoding exon; line, introns; red star, M1 mutation. (B and C) Representative images of α HA-stained (red) ASP and wing disc from homozygous *wt^{endo}* ($n = 85$) and *m1^{endo}* ($n = 79$) larvae. (D and E) Representative images of α HA-immunostained (red) ASP and wing disc from *wt^{endo}* larvae after 5 h of ex vivo culture in the absence (control; $n = 18$) and presence ($n = 29$) of Furin inhibitors. In B–E, white dashed line, ASP; blue, phalloidin-Alexa Fluor 647; arrow, t-*WT^{endo}*; arrowhead, uncleaved *WT^{endo}* or *M1^{endo}*. (F–G') Receptor-colocalized t-*WT^{endo}* and *M1^{endo}* puncta (arrow) in trans-heterozygous *btl:Cherry^{endo}/wt^{endo}* (F and F') and *btl:Cherry^{endo}/m1^{endo}* (G and G') ASP; split red channels (F' and G'). (H–I') Live images of CD8:Cherry-marked ASPs showing the long (>15 μ m) oriented ASP cytonemes (arrows) containing t-*WT^{endo}* (H and H') and *M1^{endo}* (I and I') puncta (arrowheads). (J and J') Surface α GFP^{ex} immunostaining (white) detecting *M1^{endo}* on the ASP cytoneme surfaces of *btl:cherry^{endo}/m1^{endo}* larvae; arrow and arrowhead, receptor-colocalized intracellular (bright green) and surface *M1^{endo}*, respectively. (K) Graph comparing the number of cytonemes (>15 μ m long) counted from a 60- μ m perimeter centering the ASP tip (Materials and methods) in *wt^{endo}* ($n = 28$) and *m1^{endo}* ($n = 38$). Scale bars: 20 μ m (B–G', J, and J'); 10 μ m (H–I').

had significantly higher t-*WT^{endo}* density in comparison to *M1^{endo}* (Fig. 9, N–P). Thus, Bnl cleavage in the source cells directs efficient polarized sorting of the signal to the basal signaling surface, thereby affecting intercellular signaling range and tissue morphogenesis.

Discussion

This study showed that the FGF family protein Bnl is synthesized as a proprotein and then endoproteolytically cleaved at a single site by Furin1 in the Golgi network. The cleavage ensures efficient polarized intracellular sorting of a truncated C-terminal fragment containing the FGF domain to the signaling site, where the signal is received by the ASP cytonemes for intercellular dispersal and signaling.

Limited proteolysis is one of the versatile posttranslational mechanisms that activates most, if not all, developmental signals (LeMosy, 2006). Signals including Hedgehog (Hh); Dispatched; EGF; Trunk; the TGF- β /BMP family proteins Decapentaplegic (Dpp), Screw, and Glass bottom boat (Gbb); two *Drosophila* FGFs,

Pyr and Ths; and human FGF7 were all shown to be cleaved (Lee et al., 1994; Schweitzer et al., 1995; Porter et al., 1996; K nnapuu et al., 2009, 2014; Wharton and Serpe, 2013; Constam, 2014; Johnson et al., 2015; Anderson and Wharton, 2017; Stewart et al., 2018). Although most signal cleavage is considered to activate the signal and affect the range of signaling response (K nnapuu et al., 2009, 2014; Wharton and Serpe, 2013), full-length uncleaved signals were also found to activate receptors and were shown to be secreted when expressed in cultured cells (K nnapuu et al., 2009; Sopory et al., 2010; Tokhunts et al., 2010; Tulin and Stathopoulos, 2010; Constam, 2014). Therefore, why are signals synthesized as proproteins and subsequently cleaved for their activity or dispersion?

We showed that Bnl cleavage acts as a catalytic switch that ensures its efficient polarized sorting to the basal signaling surface from where it can be taken up by the recipient cytonemes (Fig. 10). The uncleavable mutant Bnl can activate receptors but is presented on the basal surface at low levels (Fig. 9, A–M). The reduced basal presentation of uncleavable Bnl is due to its mistargeting to a far apical domain of the source cells,

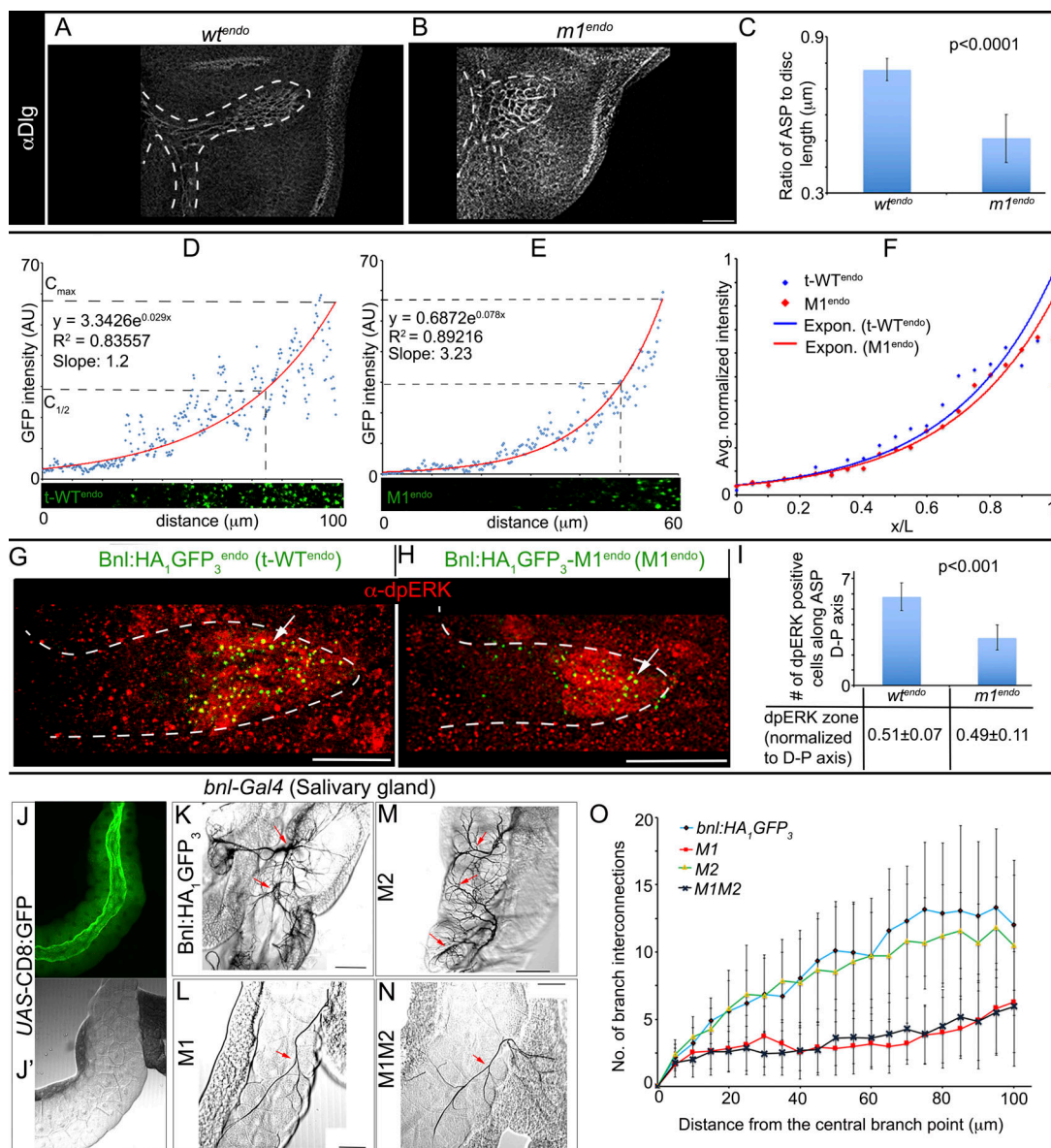


Figure 8. Bnl cleavage determines the range of gradient distribution and signaling. (A–C) Images of α Dlg immunostained (white) ASPs (white outline) and wing discs from homozygous *wt^{endo}* ($n = 52$) and *m1^{endo}* ($n = 64$) larvae (A and B); a graphical comparison (C) of their ASP length relative to the wing disc size. **(D and E)** Average intensity profiles of *t-WT^{endo}* (D, $n = 3$) and *M1^{endo}* (E, $n = 5$) along the ASP D-P axis; lower panels, examples of signal distribution along the ASP D-P axis. Red line, exponential fit trend line; C_{max} , maximum average intensity; $C_{1/2}$, $1/2 C_{max}$; slope for the trend line between C_{max} and $C_{1/2}$. **(F)** Average intensity profiles of *t-WT^{endo}* ($n = 9$) and *M1^{endo}* ($n = 12$) normalized with recipient ASP length (D-P axes; Materials and methods). **(G–I)** Images of adpERK-stained (red) ASPs from homozygous *wt^{endo}* ($n = 16$) and *m1^{endo}* ($n = 20$) larvae (G and H) and graphical comparison (I) of their nuclear dpERK-positive zones along the D-P axes; lower chart: average ratio (\pm SD) of number of dpERK-positive cells along the D-P axis to the total number of cells in the D-P axis. **(J–N)** Larval salivary glands expressing CD8:GFP, Bnl:HA1GFP3 (18), M1 (11), M2 (20), and M1M2 (18) under *bnl-Gal4* as indicated. Red arrow, central branch point. **(O)** A quantitative assessment of the frequency of terminal branching on salivary gland determined by Sholl analysis under the conditions indicated. Scale bars: 30 μ m (A, B, G, and H); 100 μ m (J–N).

which the trachea cannot access. Therefore, we predict that a pro-Bnl cleavage activates a delivery barcode for efficient target-specific intercellular dispersal. Conceptually, the cleavage ensures a signaling polarity that is relayed from within the source cells to the recipient ASP through cytonemes. Such signal barcoding for determining intercellular destination might be conserved for all signals. Consistent with this view, a similar cleavage-dependent polarized sorting mechanism was reported for Hh in *Drosophila* retinal photoreceptor neurons (Huang and

Kunes, 1996; Chu et al., 2006; Daniele et al., 2017). A complex choreography of apical and basal localization followed by the basal cytoneme-dependent dispersion of Hh was also described in *Drosophila* wing imaginal disc cells (Kornberg, 2011; Guerrero and Kornberg, 2014).

Interestingly, the efficiency of intracellular and intercellular Bnl trafficking depends on the enzymatic activity of Furl1 (Fig. 5 G and Fig. S3, A–D). Although Bnl expression is spatially restricted in tissues, the molecular machinery that cleaves Bnl

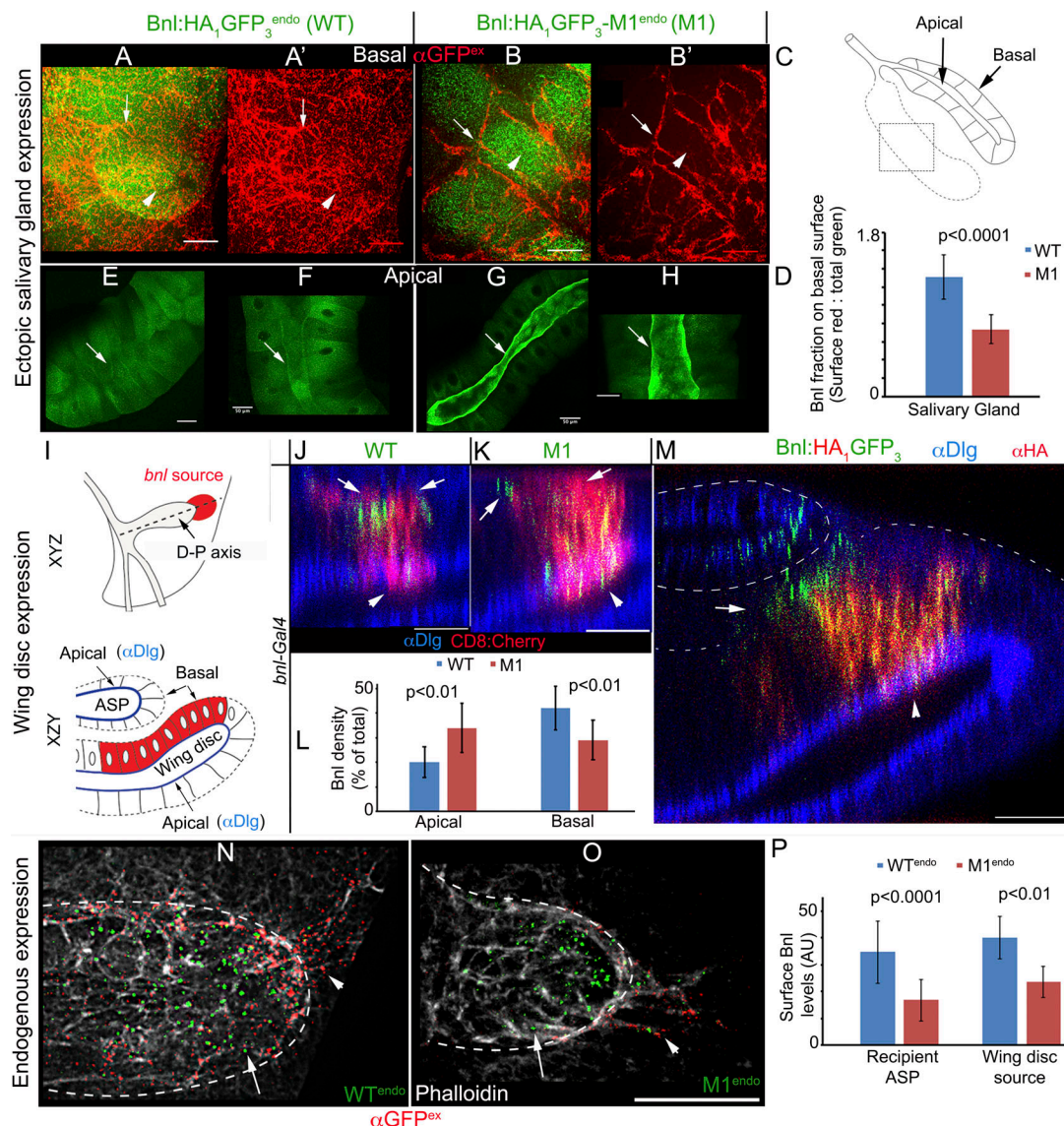


Figure 9. Cleavage ensures polarized Bnl sorting to the basal cell surface for signaling. (A–C) High-magnification (40×) images of the exposed basal surfaces (arrowhead) of salivary glands expressing WT or M1 under *bnl-Gal4* from an area schematically shown in C. Red, surface $\alpha\text{GFP}^{\text{ex}}$ immunostaining; arrow, cell junction. (D) Graph comparing fractions (red surface stain/total GFP) of overexpressed WT ($n = 12$) and M1 ($n = 10$) that got externalized on the salivary gland surface. (E–H) Images of sagittal sections of salivary glands expressing WT and M1 under *bnl-Gal4*. Arrow, apical lumen. (I) Drawings depicting the ASP D–P axis (dashed line; upper panel) and an XYZ section along the D–P axis (lower panel) showing the tubular ASP and disc epithelia as shown in J–M. (J and K) Sagittal sections of αDlg immunostained (blue, sub-apical marker) wing disc and ASP when the disc *bnl* source coexpressed CD8:Cherry with either the WT or M1 construct under *bnl-Gal4*. Arrow, basal side; arrowhead, apical side. (L) Graph comparing apical and basal percentage of WT and M1 relative to the total amount in the disc source. $n = 24$ (WT) and 32 (M1). (M) Maximum projections of mid- and para-sagittal sections within $\sim 3 \mu\text{m}$ of mid-Y of an αDlg (blue) and αHA (red) stained wing-disc/ASP, where *bnl-Gal4* expressed *Bnl:HA₁GFP₃*. Arrow, truncated *Bnl:GFP₃*; white dashed line, ASP and wing disc; arrowhead, apical lumen of wing disc. (N–P) Comparison (graph in P) of levels of t-WT^{endo} ($n = 17$) and M1^{endo} ($n = 33$) on the surface of the disc source and ASP (dashed line). Red and arrowhead, detergent-free αGFP -staining; arrow, intracellular puncta; white staining, phalloidin-Alexa Fluor 647. Scale bars: 50 μm (E–H); 20 μm (all other panels).

exists even in salivary glands that do not normally express Bnl. This might reflect the broad range of Fur1 expression, as reported in several studies (Roebroek et al., 1992, 1993; Künnapuu et al., 2009; Nichols and Weinmaster, 2010; Johnson et al., 2015). Alternatively, different types of cells might express different *furin/PC* genes that can act redundantly. Furins are known to be regulated enzymes that autoactivate in a Ca^{2+} -dependent manner during their intracellular trafficking (Thomas, 2002). How

and when the Furin activation pathway might intersect with the pro-Bnl sorting itinerary is unknown. We also do not know why a truncated Bnl is targeted only to the basal cell surface. Recently, the trans-Golgi cargo receptor AP-1 γ , a component of the Clathrin AP-1 complex, was shown to be necessary for Bnl trafficking to the basolateral membranes of *bnl*-expressing flight muscle cells (Peterson and Krasnow, 2015). It is possible that Bnl cleavage unmasks the cargo-receptor binding site. The current

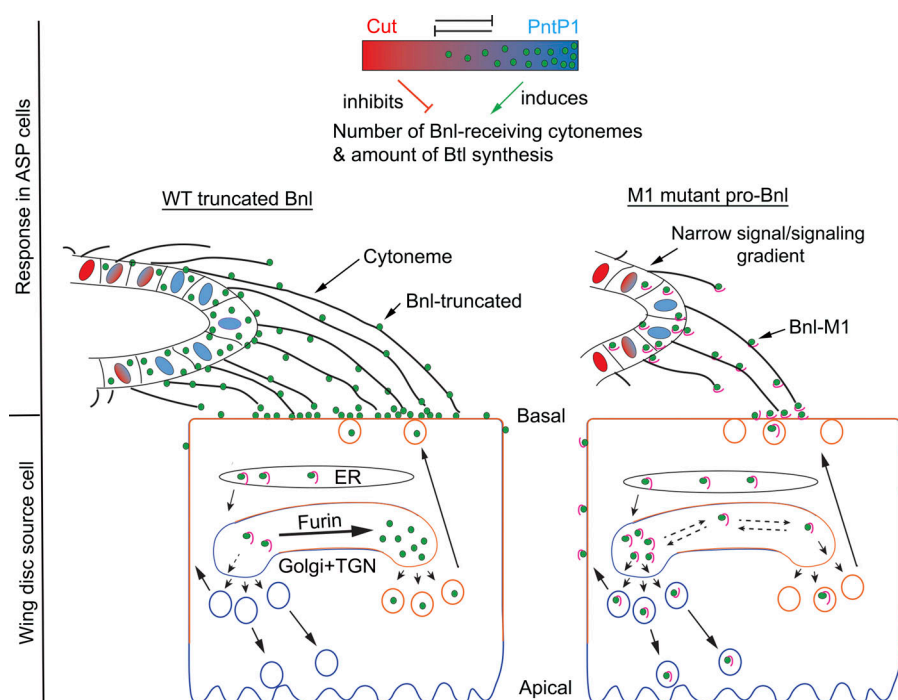


Figure 10. Proposed model for the role of Bnl cleavage in determining signaling range. Pro-Bnl is cleaved by Furin1 in the Golgi into a truncated-Bnl, which, through an unknown process, is asymmetrically sorted to the basal surface of the source cells. In the absence of cleavage, mutant Bnl-M1 molecules traffic randomly and are mostly sequestered at a distant apical domain, reducing their basal availability. The ASP, which is present on the basal side of the source, extends cytonemes to directly receive Bnl from the basal surface of the source cells. High Bnl levels/signaling in the ASP induce PntP1, which induces Bnl-receiving cytoneme formation. Lower Bnl uptake in cells further from the source induces Cut, which suppresses Bnl-receiving cytoneme formation. Cut and PntP1 feedback inhibit each other's expression, thereby generating a Bnl gradient that adopts recipient ASP-specific shapes (Du et al., 2018a). Consequently, reduced Bnl-M1 availability results in only a few ASP cells extending Bnl-receiving cytonemes, leading to a restricted range of signal distribution and stunted ASP growth.

knowledge of intracellular Bnl/FGF targeting is rudimentary and needs to be elucidated in the future.

Our findings revealed that although Bnl cleavage is intracellular, it plays an important role in determining the range of cytoneme-mediated intercellular Bnl dispersal. Insights on how this intracellular event might influence the range of cytoneme-dependent dispersal came from our earlier study (Du et al., 2018a). As illustrated in Fig. 10, high to low levels of Bnl signaling activate two counteracting feedback loops operating from the opposite poles of the ASP, which help to establish the zones of corresponding high to low number of Bnl-receiving cytonemes along the ASP epithelium. The consequence is a systemic self-regulatory process, where the number of Bnl-receiving cytonemes produced by ASP cells is determined by the amount of Bnl received by the cells through cytonemes, giving rise to the recipient ASP-specific Bnl gradient shapes. Therefore, the intracellular cleavage and polarized sorting pathway that modulate Bnl availability on the basal surface of source cells can determine the spatial range of cytoneme formation, signal dispersion, and signaling. These results suggest an intricate coordination of the intracellular events in the source and recipient cells with the intercellular cytoneme-mediated dispersal, which together can precisely shape signal gradients and tissue patterns.

Materials and methods

Drosophila strains and genetic crosses

All crosses were incubated at 25°C. The following strains were used in this study: *UAS-bnlRNAi* (34572), *fur1-LacZ* (10341), *UAS-fur1RNAi* (25837), *UAS-fur1RNAi* (42481), *UAS-fur1RNAi* (41914), *UAS-fur2RNAi* (51743), *UAS-fur2RNAi* (42577), *UAS-fur1* (63077) (from Bloomington Stock Center); *UAS_{attB}-Bnl:GFP₁*, *UAS_{attB}-Bnl:*

GFP₂, *UAS_{attB}-Bnl:GFP₃*, *UAS_{attB}-Bnl:GFP₄*, *UAS_{attB}-Bnl:HA₁*, *UAS_{attB}-Bnl:HA₂*, *UAS_{attB}-Bnl:HA₃*, *UAS_{attB}-Bnl:HA₄* (gifts from Kornberg lab); *fur2-Gal4* (NP 4074) (from Kyoto DGGR); *UAS-CD8:GFP*, *UAS-CD8:Cherry*, *btl-Gal4*, *bnl-Gal4* (Roy et al., 2014); *bnl:gfp^{endo}*, *btl:cherry^{endo}* (Du et al., 2018a); and *UAS-Bnl:GFP₁*, *UAS-Bnl:HA₁*, *UAS-Bnl:GFP₂*, *UAS-Bnl:GFP₃*, *UAS-Bnl:HA₃*, *UAS-Bnl:GFP₄*, *UAS-Bnl:HA₁GFP₃*, *UAS-Bnl:HA₁GFP₃-M1*, *UAS-Bnl:HA₁GFP₃-M2*, *UAS-Bnl:HA₁GFP₃-M1M2*, *bnl:HA₁GFP₃^{endo}*, *bnl:HA₁GFP₃-M1^{endo}* (this study).

Generation of transgenic *Drosophila* lines

UAS-bnl:GFP and *UAS-bnl:HA* variants

Each of the four Bnl:GFP variants contained an HA-tag upstream to a GFP tag at a single internal site. Bnl:GFP₁ contained both HA and GFP tags in tandem inserted between amino acids RSSLVPSAVS⁸⁷ and E⁸⁸RSVNQPT. Bnl:GFP₂ contained the tags inserted between amino acids SNLDRNERST²⁰⁶ and V²⁰⁷PQSHLAWTS. Bnl:GFP₃ contained the tags inserted between amino acids KAPPHCSSNT⁴³² and S⁴³³GSSSSISS. Bnl:GFP₄ contained the tags between amino acids MSSGEEQDQN⁷⁰¹ and D⁷⁰²QDQEQSDPGE. Previously, transgenic *Drosophila* lines harboring the Bnl:GFP₃ construct at various *attP* loci in the second and fourth chromosomes did not show any detectable Bnl:GFP₃ expression when driven by *bnl-Gal4*. Therefore, we subcloned the Bnl:GFP constructs into the pUAST vector from the original pUAST-attB constructs and resorted to the random P-element-based transgenesis to avoid any positional effects on Bnl:GFP expression. A summary of characterization of different transgenic lines is presented in Table S2.

UAS-bnl:HA₁GFP₃

UAS-bnl:HA₁GFP₃ contained an HA-tag at site 1 (between 87 and 88 amino acid residues of the original protein) and a superfolder

GFP (Pédélec et al., 2006) at site 3 (between 432 and 433 residues of the original protein). The construct was generated by overlap extension PCR of three fragments using primers (Table S1): the N-terminal HA-tagged part, the C-terminal Bnl coding region (amplified from the pUAST-attB-Bnl:HA₁), and the middle sfGFP region from a sfGFP-containing construct (Addgene). The final 3,060-bp PCR product was cloned into the pCR-Blunt II-TOPO vector. The fully sequence-verified insert was subcloned into the pUAST vector at the BglII and XbaI sites. UAS-bnl:HA₁GFP₃ was used for analysis in S2 cells and for P-element-mediated germline transformation and transgenesis.

UAS-bnl:HA₁GFP₃ mutants

The M1 and M2 variants of Bnl:HA₁GFP₃ contained the following cleavage site mutations: M1, (R/G)TE(R/G)SI(R/G); M2, (R/G)NE(R/G). These mutant constructs were created using overlap extension PCR with the Bnl:HA₁GFP₃ construct as a template. The primers used are shown in Table S1. The final assembled PCR product was cloned into the pCR-Blunt II-TOPO vector. The sequence-verified constructs were subcloned into the BglII and XbaI sites of the pUAST vector for either analysis in S2 cell culture or for P-element-mediated germline transformation and transgenesis.

UAS-bnl:HA₁GFP₄ and UAS-bnl:GFP₁HA₄

UAS-bnl:HA₁GFP₄ was cloned using overlap extension PCR to insert a GFP tag at site 4 of Bnl:HA₁. Similarly, UAS-bnl:GFP₁HA₄ was cloned using overlap extension PCR to insert a GFP at site 1 of Bnl:HA₄. The primers used are listed in Table S1. These constructs were verified and used in S2 cell culture analyses. P-element based transgenesis was performed as described earlier (Du et al., 2017). Various transgenic lines generated are described in Table S2.

CRISPR/Cas9-based genome editing

The bnl:HA₁GFP₃^{endo} and bnl:HA₁GFP₃-M1^{endo} mutant alleles were generated by in-frame insertion of an HA-tag into the first coding exon of a previously characterized bnl:sfGFP₃^{endo} allele (Du et al., 2018a) using CRISPR/Cas9-based genome editing following previously described protocols (Du et al., 2017, 2018b). The bnl:HA₁GFP₃-M1 mutant allele includes the HA₁ tag as well as mutations of three arginines (R) to glycines (G) at PCS1 that starts 82 amino acids upstream of the conserved FGF domain. For targeting Cas9-based double-stranded break near tag site 1, a guide RNA (BnlHA1gRNA, 5'-CTACGTTCACTCACTGCGCTCGG-3'; underlined bases represent the PAM site) with zero off targets in the fly genome was cloned by ligating two annealed complimentary oligonucleotides into the pCFD3 vector (Table S1).

The replacement donors, pDonor-bnl:HA₁GFP₃ and pDonor-bnl:HA₁GFP₃-M1, were designed and generated following Du et al. (2017). These constructs contained either HA₁ or the HA₁-M1 mutations flanked by ~1-kb long 5' and 3' arms that are homologous to the genomic sequence flanking tag site 1. Both 5' and 3' homology arms were PCR-amplified from genomic DNA from the nos-Cas9;bnl:GFP₃^{endo} parent fly, sequence verified, and assembled together into the pUC19 vector using Gibson Assembly (primers in Table S1). To prevent retargeting of the gRNA/Cas9 to the edited genome, a synonymous mutation was

introduced into the replacement cassette near the PAM sequence via the primers used for amplification (Table S1). The constructs were fully sequenced before germline injection.

The gRNA-expressing vector and the respective replacement donor vector were coinjected into the germline cells of nos-Cas9; bnl:sfGFP₃^{endo} embryos. For each genome-editing experiment, a stepwise crossing strategy (Du et al., 2018b) was followed to obtain G0-F2 progenies and establish individual fly lines for screening. The desired "ends-out" homologous directed repair (HDR) was screened for by a three-step PCR-based strategy (see primers in Table S1), followed by sequencing and analyses of tissue-specific expression patterns of the tagged genes under a confocal microscope. The efficiency of genome editing-based generation of the two different genotypes and their phenotypes were summarized in Table S4. During generation of bnl:HA₁GFP₃-M1^{endo} several lines were obtained that had only the HA₁ insertion without the M1 mutation. We predicted that the HDR had taken place somewhere between the HA₁ tag site and M1 mutation sites (219 bases apart). These lines were fully sequence verified and found to have normal tissue expression. Therefore, these lines were considered as bnl:HA₁GFP₃^{endo} lines (see Table S4). For subsequent analyses, we used a wt^{endo} and an m1^{endo} line derived from the same genome-editing experiment. The wt^{endo} F4-14 line and m1^{endo} F4-9 line used in this study were fully sequence verified and established after outcrossing as previously described (Du et al., 2018a).

Synthesis of double-stranded RNA (dsRNA) for gene knockdown in S2 cells

dsRNA was synthesized by PCR from genomic DNA isolated from S2 cells following a previously described protocol (Künnapu et al., 2009). The following PCR primers were used to synthesize the T7 transcription template carrying the T7 promoter sequence at their 5' ends: fur1: forward, 5'-TAATAC GACTCACTATAGGGACGCAAAGATCCTCTGTGGCA-3'; reverse, 5'-TAATACGACTCACTATAGGGACATTGCTCCCGGAAGTGC-3'; fur2: forward, 5'-TAATACGACTCACTATAGGGACGCTAGAGG CCAATCCGGAA-3'; reverse, 5'-TAATACGACTCACTATAGGGA CCCTTCTCGCCCCAAAAGTG-3'. dsRNA against fur1 or fur2 were synthesized using the MEGAscript RNAi Kit (Thermo Fisher Scientific).

FISH

To probe for fur1 and fur2 mRNA, the desired probe regions of 540 and 552 bp were PCR amplified with primers (Table S1) from respective cDNAs and cloned using Gibson assembly into pSPT18 vector. The vector was linearized, and the RNA probe was prepared using the DIG-RNA Labeling Kit (Roche) according to the manufacturer's protocol. RNA in situ hybridization on third-instar larval tissues was performed as previously described (Du et al., 2017). Hybridized probes were detected using α-Dig antibody followed by immunofluorescence with Alexa Fluor 647-conjugated secondary antibody.

Cell culture assay

S2 cells were cultured in 25-cm² flasks using Shields and Sang M3 insect media (Sigma-Aldrich). For transfection, when cells

were ~90% confluent, the medium was removed and 6 ml of fresh M3 medium was added to the flask. Cells were gently resuspended by pipetting and added to a 12-well plate with 1 ml of cells per well. After 2 h, once the cells had adhered to the bottom of the well, the M3 media was replaced with 1 ml serum-free M3 medium, and the cells were transfected with 1 µg of each DNA using Lipofectamine 2000 following the manufacturer's protocol. After 16 h, the serum-free medium was replaced with 1 ml M3 medium containing serum. For experiments with *furin RNAi*, 5 µg of dsRNA was used for transfection. Under all conditions, transient expression was examined 2–3 d after transfection.

Ex vivo organ culture and Furin inhibitor assay

Ex vivo culturing of wing discs was performed in WM1 medium as described in [Du et al. \(2017\)](#). The discs were removed from a single pool of culture after 0, 5, and 16 h of incubation at 25°C, followed by fixation and αHA immunostaining of the tissues. For the Furin inhibition assay, late third instar larval tissues were ex vivo cultured in 2 ml of WM1 medium in the presence or absence of a cocktail of Furin inhibitor I and II (50 µM final concentration each; Calbiochem; 344930 and 344931) following recommended concentrations in [Johnson et al. \(2015\)](#). The live tissues were incubated for 1, 2.5, or 5 h. Following incubation, the carcasses were transferred to a centrifuge tube, rinsed three times with 1× PBS, and fixed in 4% PFA before αHA immunostaining.

Protein analyses

S2 cells were harvested 3 d posttransfection, and the cell pellets were washed several times in 1× PBS. The pellet was resuspended in 70 µl RIPA cell lysis buffer (Sigma-Aldrich) in the presence of a cocktail of protease inhibitors (Roche) and kept for 15 min at 4°C. An equal volume of lysed cells was combined with 2× Sample Buffer, heated at 95°C for 5 min, and loaded onto a 10% SDS-PAGE minigel. The gel was run at 50 V for 10 min for stacking and then at 200 V until the desired amount of separation occurred. Proteins were transferred from the gel to a PVDF membrane using Transblot Turbo (Bio-Rad). A standard protocol was followed to perform Western blot analyses using primary antibodies: αGFP (1:1,000) or αHA (1:1,000) and HRP-conjugated secondary antibody. The HRP activity was detected with ECL substrate (GE) and imaged (Fuji LAS3000).

Immunostaining

Standard and detergent-free immunostaining protocols were as previously described ([Du et al., 2017](#)). The following antibodies were used in this study: α-Discs large (1:100; DSHB); α-HA (1:1,000); α-dpERK (1:100; Cell Signaling); α-GFP (1:3,000 extracellular; Abcam); and α-PH3 (1:2,000; Cell Signaling). Alexa Fluor-conjugated secondary antibodies (1:1,000; Molecular Probes) were used for immunofluorescence detection. Phalloidin-conjugated Alexa Fluor 647 was often used for marking cell outlines.

Microscopic imaging

For live imaging, wing imaginal discs and their associated trachea were prepared following [Roy et al. \(2014\)](#). Images were obtained as previously described ([Du et al., 2018a](#)) using a Leica

SP5X with HyD detector or an CSUX1 Yokogawa spinning disc confocal equipped with an Andor iXon897 EMCCD camera. The images were processed and analyzed with Fiji. Maximum-intensity projections of sections were shown for most images. All images were obtained using 40× objective in the microscopes, except for [Fig. 8 \(J–N\)](#), which used a 20× objective. All XZY images were obtained using the Leica SP5X with a 40× objective for S2 cells and 20× objective for wing discs.

Analysis of ASP size

ASP length was measured from the TC along their longest (major) D–P axis to the ASP tip. The disc size was determined by measuring from the TC, along the ASP major axis to the edge of the disc. A ratio of the ASP:disc size was used to compare different genotypes and conditions ([Figs. 5 J'](#) and [8 C](#)).

Sholl analysis for terminal branching

Salivary glands were gently dissected out from fixed larval tissues overexpressing different cleaved and uncleaved variants of Bnl and imaged under transmitted light to visualize tracheal invasion. In WT overexpressing tissue, the terminal tracheal branches ramified radially from a preexisting central branch point. Due to its morphological resemblance with neuronal dendritic arbors, we employed Sholl analysis ([Binley et al., 2014](#)) using Fiji to measure the frequency of terminal branching. The analysis created 20 concentric circles in increments of 5-µm radius from the point of origin up to 100 µm and counted the number of times any tracheal branch crossed these circles. These values were averaged across several samples and compared between the different Bnl variants expressed in the salivary gland.

Quantitative analyses of fluorescence intensities

For Bnl levels, all fluorescent intensity measurements were background corrected. 3D image stacks representing only either the wing disc sections or the ASP were transformed into 2D by maximum-intensity projections. The density of fluorescence intensity was measured from a selected region of interest (ROI) of the 2D images, outlining the either Bnl source cells or the recipient ASP ([Figs. 2 I, 6 G, and S5 C](#)). For the recipient ASP, the ROI encompassed the distal tip of the ASP (a region with ~3–4-cell diameter that received the maximum Bnl from the source). Likewise, the density of the surface-localized Bnl:GFP variants, probed by αGFP immunostaining ([Fig. 9 P](#)), was measured from selected ROIs on the maximum-intensity projections of the relevant optical sections encompassing either the ASP or wing disc source. For [Fig. 9 D](#), the ROIs represented each salivary gland cell including the cell junctions, and the density of the red and green channel intensities were measured from the maximum-intensity projections of optical sections within the 5-µm Z-stack from the most basal surface. The ratio of surface GFP (red) to total GFP (green) was expected to be less than one. However, some average ratios were slightly greater than one, probably due to the immunofluorescent signal amplification of the surface-exposed proteins obtained through αGFP immunostaining. Second, as reported earlier ([Du et al., 2018a](#)), the surface exposed GFP was rapidly quenched, reducing its levels of

detection on the cell surface. For Fig. 9 (J–L), ROIs representing the basal or apical part of the source cells were selected from maximum-intensity projections of the XZY sections. GFP intensities measured from the ROIs were normalized to the total intensity from the total source cell area.

For colocalization analyses in S2 cells (Figs. 3 H and 5 E), maximum-intensity projections of approximately four to five stacks around the center of the cell were produced. An I_{corr} value was obtained using the Colocalization Colormap plugin of Fiji to determine the degree of colocalization of two selected channels (HA immunostain and GFP).

Gradients of intensities of Bnl:GFP variants in the ASP (Fig. 8, D–F) were obtained along the ASP D–P axes as reported earlier (Du et al., 2018a). For Fig. 8 F, gradients were measured from homozygous wt^{endo} ($n = 9$) or $M1^{endo}$ ($n = 12$) ASPs. Each position (x) within an ASP was normalized by length of the ASP (L) to obtain x/L , the x-axis of the plot. Similarly, GFP intensity was normalized by dividing each intensity value in a single sample by the highest intensity value from that sample for the y-axis. Normalized intensity values from each sample were taken at 0.05 x/L increments from 0 to 1 (i.e., 21 data points from each sample). The normalized intensity values from each group (WT or M1) were averaged together and plotted along the x/L axis.

Cytoneme analysis

ASP cytoneme number was quantitated microscopically as previously described (Roy et al., 2011, 2014). In brief, cytonemes $>15 \mu\text{m}$ in length that extended from a $60\text{-}\mu\text{m}$ total perimeter region ($30 \mu\text{m}$ from the tip of the ASP in both directions) were counted.

Statistical analyses

Statistical significance was determined with two-tailed t tests or a one-way ANOVA followed by Tukey's honestly significant different (HSD) tests. All P values in the legends were obtained using a t test, unless otherwise stated.

Online supplemental material

Fig. S1 shows additional images comparing Bnl:GFP₁ and Bnl:GFP₃ expression and dispersion. Fig. S2 shows additional biochemical and cell-biological evidence of Bnl cleavage. Fig. S3 shows ASP phenotypes due to *bnl* and *fur* knockdown in the disc *bnl* source and expression analyses of *fur* genes. Fig. S4 shows additional examples of localization and activity of WT^{endo} and M1^{endo} in the ASP. Fig. S5 shows cleavage of Bnl:HA₁GFP₃ in the salivary gland, a quantitative analysis performed to identify lines of Bnl:HA₁GFP₃ variants that expressed at equivalent levels, and a graph comparing the percentage of WT and M1 proteins on the surface of the wing disc cells that overexpressed the proteins. Video 1 shows the organization of the ASP and wing disc *bnl*-source. Video 2 shows the Bnl:GFP₃ distribution in a 3D ASP section. Video 3 shows the lack of Bnl:GFP₁ in ASP 3D images. Videos 4 and 5 show the spatial distribution of cleaved Bnl portions in XYZ and XZY S2 cell sections. Video 6 shows the spatial distribution of the uncleaved M1 mutant Bnl in a S2 cell. Video 7 shows the spatial distribution of the uncleaved M1 mutant Bnl in the wing disc-ASP. Table S1 lists primers used in this study. Table S2 lists transgenic *Drosophila* lines created for

this study and their analyses. Table S3 lists phenotypic analyses of *fur* expression knockdown by various RNAi lines. Table S4 shows the efficiency of generation of *bnl*:HA₁sGFP₃ and *bnl*:HA₁sGFP₃-M1 mutant *Drosophila* lines using CRISPR/Cas9.

Acknowledgments

We thank Dr. T.B. Kornberg for the Bnl:GFP constructs and all his mentorship and support; the Bloomington Stock Center for *Drosophila* lines; Developmental Studies Hybridoma Bank for antibodies; Drs. N.W. Andrews and T.B. Kornberg for comments on the manuscript; and A.E. Beaven for assistance in the CBMG Imaging Core.

This study was funded by the National Institutes of Health: grants K99/R00HL114867 and R35GM124878 to S. Roy. A. Sohr received a one-year fellowship from a Cell and Molecular Biology Training Grant (T32-GM080201).

The authors declare no competing financial interests.

Author contributions: L. Lin generated the Bnl:GFP1-4 constructs; A. Sohr, L. Du, R. Wang, and S. Roy conducted the experiments; S. Roy designed the project and supervised the work; S. Roy, A. Sohr, R. Wang, and L. Du wrote the paper.

Submitted: 25 October 2018

Revised: 30 January 2019

Accepted: 5 February 2019

References

- Akiyama, T., and M.C. Gibson. 2015. Morphogen transport: theoretical and experimental controversies. *Wiley Interdiscip. Rev. Dev. Biol.* 4:99–112. <https://doi.org/10.1002/wdev.167>
- Anderson, E.N., and K.A. Wharton. 2017. Alternative cleavage of the bone morphogenetic protein (BMP), Gbb, produces ligands with distinct developmental functions and receptor preferences. *J. Biol. Chem.* 292: 19160–19178. <https://doi.org/10.1074/jbc.M117.793513>
- Binley, K.E., W.S. Ng, J.R. Tribble, B. Song, and J.E. Morgan. 2014. Sholl analysis: a quantitative comparison of semi-automated methods. *J. Neurosci. Methods.* 225:65–70. <https://doi.org/10.1016/j.jneumeth.2014.01.017>
- Briscoe, J., and S. Small. 2015. Morphogen rules: design principles of gradient-mediated embryo patterning. *Development.* 142:3996–4009. <https://doi.org/10.1242/dev.129452>
- Chang, W.-L., S. Yamamoto, M. Jaiswal, V. Bayat, B. Xiong, K. Zhang, H. Sandoval, G. David, S. Gibbs, H.-C. Lu, et al. 2014. *Drosophila* Tempura, a novel protein prenyltransferase α subunit, regulates notch signaling via Rab1 and Rab11. *PLoS Biol.* 12:e1001777. <https://doi.org/10.1371/journal.pbio.1001777>
- Christian, J.L. 2012. Morphogen gradients in development: from form to function. *Wiley Interdiscip. Rev. Dev. Biol.* 1:3–15. <https://doi.org/10.1002/wdev.2>
- Chu, T., M. Chiu, E. Zhang, and S. Kunes. 2006. A C-terminal motif targets Hedgehog to axons, coordinating assembly of the *Drosophila* eye and brain. *Dev. Cell.* 10:635–646. <https://doi.org/10.1016/j.devcel.2006.03.003>
- Constam, D.B. 2014. Regulation of TGF β and related signals by precursor processing. *Semin. Cell Dev. Biol.* 32:85–97. <https://doi.org/10.1016/j.semcdb.2014.01.008>
- Daniele, J.R., T. Chu, and S. Kunes. 2017. A novel proteolytic event controls Hedgehog intracellular sorting and distribution to receptive fields. *Biol. Open.* 6:540–550. <https://doi.org/10.1242/bio.024083>
- Du, L., A. Zhou, A. Patel, M. Rao, K. Anderson, and S. Roy. 2017. Unique patterns of organization and migration of FGF-expressing cells during *Drosophila* morphogenesis. *Dev. Biol.* 427:35–48. <https://doi.org/10.1016/j.ydbio.2017.05.009>
- Du, L., A. Sohr, G. Yan, and S. Roy. 2018a. Feedback regulation of cytoneme-mediated transport shapes a tissue-specific FGF morphogen gradient. *eLife.* 7:e38137. <https://doi.org/10.7554/eLife.38137>

- Du, L., A. Zhou, A. Sohr, and S. Roy. 2018b. An efficient strategy for generating tissue-specific binary transcription systems in *Drosophila* by genome editing. *J. Vis. Exp.* doi: 10.3791/58268. <https://doi.org/10.3791/58268>
- Duckert, P., S. Brunak, and N. Blom. 2004. Prediction of proprotein convertase cleavage sites. *Protein Eng. Des. Sel.* 17:107–112. <https://doi.org/10.1093/protein/gzh013>
- Guerrero, I., and T.B. Kornberg. 2014. Hedgehog and its circuitous journey from producing to target cells. *Semin. Cell Dev. Biol.* 33:52–62. <https://doi.org/10.1016/j.semcdb.2014.06.016>
- Huang, Z., and S. Kunes. 1996. Hedgehog, transmitted along retinal axons, triggers neurogenesis in the developing visual centers of the *Drosophila* brain. *Cell*. 86:411–422. [https://doi.org/10.1016/S0092-8674\(00\)80114-2](https://doi.org/10.1016/S0092-8674(00)80114-2)
- Jarecki, J., E. Johnson, and M.A. Krasnow. 1999. Oxygen regulation of airway branching in *Drosophila* is mediated by branchless FGF. *Cell*. 99: 211–220. [https://doi.org/10.1016/S0092-8674\(00\)81652-9](https://doi.org/10.1016/S0092-8674(00)81652-9)
- Jaskolski, F., C. Mulle, and O.J. Manzoni. 2005. An automated method to quantify and visualize colocalized fluorescent signals. *J. Neurosci. Methods*. 146:42–49. <https://doi.org/10.1016/j.jneumeth.2005.01.012>
- Johnson, T.K., M.A. Henstridge, A. Herr, K.A. Moore, J.C. Whisstock, and C.G. Warr. 2015. Torso-like mediates extracellular accumulation of Furin-cleaved Trunk to pattern the *Drosophila* embryo termini. *Nat. Commun.* 6:8759. <https://doi.org/10.1038/ncomms9759>
- Kornberg, T.B. 2011. Barcoding Hedgehog for intracellular transport. *Sci. Signal.* 4:pe44. <https://doi.org/10.1126/scisignal.2002447>
- Kornberg, T.B. 2016. A Path to Pattern. *Curr. Top. Dev. Biol.* 116:551–567. <https://doi.org/10.1016/bs.ctdb.2015.11.026>
- Künnapu, J., I. Björkgren, and O. Shimmi. 2009. The *Drosophila* DPP signal is produced by cleavage of its proprotein at evolutionary diversified furin-recognition sites. *Proc. Natl. Acad. Sci. USA*. 106:8501–8506. <https://doi.org/10.1073/pnas.0809885106>
- Künnapu, J., P.M. Tauscher, N. Tiisanen, M. Nguyen, A. Löytynoja, K. Arora, and O. Shimmi. 2014. Cleavage of the *Drosophila* screw prodomain is critical for a dynamic BMP morphogen gradient in embryogenesis. *Dev. Biol.* 389:149–159. <https://doi.org/10.1016/j.ydbio.2014.02.007>
- Lee, J.J., S.C. Ekker, D.P. von Kessler, J.A. Porter, B.I. Sun, and P.A. Beachy. 1994. Autoproteolysis in hedgehog protein biogenesis. *Science*. 266: 1528–1537. <https://doi.org/10.1126/science.7985023>
- LeMosy, E.K. 2006. Proteolytic regulatory mechanisms in the formation of extracellular morphogen gradients. *Birth Defects Res. C Embryo Today*. 78:243–255. <https://doi.org/10.1002/bdrc.20074>
- Nichols, J.T., and G. Weinmaster. 2010. *Proteolytic Activation of Notch Signaling: Roles for Ligand Endocytosis and Mechanotransduction*. Vol. 2. Second edition. Elsevier Inc., New York; 7 pp. <https://doi.org/10.1016/B978-0-12-374145-5.00232-1>
- Ochoa-Espinosa, A., and M. Affolter. 2012. Branching morphogenesis: from cells to organs and back. *Cold Spring Harb. Perspect. Biol.* 4:a008243. <https://doi.org/10.1101/cshperspect.a008243>
- Ohshiro, T., Y. Emori, and K. Saigo. 2002. Ligand-dependent activation of breathless FGF receptor gene in *Drosophila* developing trachea. *Mech. Dev.* 114:3–11. [https://doi.org/10.1016/S0925-4773\(02\)00042-4](https://doi.org/10.1016/S0925-4773(02)00042-4)
- Pédélecq, J.-D., S. Cabantous, T. Tran, T.C. Terwilliger, and G.S. Waldo. 2006. Engineering and characterization of a superfolder green fluorescent protein. *Nat. Biotechnol.* 24:79–88. <https://doi.org/10.1038/nbt1172>
- Peterson, S.J., and M.A. Krasnow. 2015. Subcellular trafficking of FGF controls tracheal invasion of *Drosophila* flight muscle. *Cell*. 160:313–323. <https://doi.org/10.1016/j.cell.2014.11.043>
- Porter, J.A., K.E. Young, and P.A. Beachy. 1996. Cholesterol modification of hedgehog signaling proteins in animal development. *Science*. 274: 255–259. <https://doi.org/10.1126/science.274.5285.255>
- Ramírez-Weber, F.A., and T.B. Kornberg. 1999. Cytonemes: cellular processes that project to the principal signaling center in *Drosophila* imaginal discs. *Cell*. 97:599–607. [https://doi.org/10.1016/S0092-8674\(00\)80771-0](https://doi.org/10.1016/S0092-8674(00)80771-0)
- Roebroek, A.J., J.W. Creemers, I.G. Pauli, U. Kurzik-Dumke, M. Rentrop, E.A. Gateff, J.A. Leunissen, and W.J. Van de Ven. 1992. Cloning and functional expression of Dfurin2, a subtilisin-like proprotein processing enzyme of *Drosophila melanogaster* with multiple repeats of a cysteine motif. *J. Biol. Chem.* 267:17208–17215.
- Roebroek, A.J., J.W. Creemers, I.G. Pauli, T. Bogaert, and W.J. Van de Ven. 1993. Generation of structural and functional diversity in furin-like proteins in *Drosophila melanogaster* by alternative splicing of the Dfur1 gene. *EMBO J.* 12:1853–1870. <https://doi.org/10.1002/j.1460-2075.1993.tb05834.x>
- Roy, S., F. Hsiung, and T.B. Kornberg. 2011. Specificity of *Drosophila* cytonemes for distinct signaling pathways. *Science*. 332:354–358. <https://doi.org/10.1126/science.1198949>
- Roy, S., H. Huang, S. Liu, and T.B. Kornberg. 2014. Cytoneme-mediated contact-dependent transport of the *Drosophila* decapentaplegic signaling protein. *Science*. 343:1244624. <https://doi.org/10.1126/science.1244624>
- Sato, M., and T.B. Kornberg. 2002. FGF is an essential mitogen and chemo-attractant for the air sacs of the *drosophila* tracheal system. *Dev. Cell*. 3: 195–207. [https://doi.org/10.1016/S1534-5807\(02\)00202-2](https://doi.org/10.1016/S1534-5807(02)00202-2)
- Schweitzer, R., M. Shaharabany, R. Seger, and B.Z. Shilo. 1995. Secreted Spitz triggers the DER signaling pathway and is a limiting component in embryonic ventral ectoderm determination. *Genes Dev.* 9:1518–1529. <https://doi.org/10.1101/gad.9.12.1518>
- Sopory, S., S. Kwon, M. Wehrli, and J.L. Christian. 2010. Regulation of Dpp activity by tissue-specific cleavage of an upstream site within the prodomain. *Dev. Biol.* 346:102–112. <https://doi.org/10.1016/j.ydbio.2010.07.019>
- Stewart, D.P., S. Marada, W.J. Bodeen, A. Truong, S.M. Sakurada, T. Pandit, S. M. Pruetz-Miller, and S.K. Ogden. 2018. Cleavage activates dispatched for Sonic Hedgehog ligand release. *eLife*. 7:e31678. <https://doi.org/10.7554/eLife.31678>
- Sutherland, D., C. Samakovlis, and M.A. Krasnow. 1996. branchless encodes a *Drosophila* FGF homolog that controls tracheal cell migration and the pattern of branching. *Cell*. 87:1091–1101. [https://doi.org/10.1016/S0092-8674\(00\)81803-6](https://doi.org/10.1016/S0092-8674(00)81803-6)
- Thomas, G. 2002. Furin at the cutting edge: from protein traffic to embryogenesis and disease. *Nat. Rev. Mol. Cell Biol.* 3:753–766. <https://doi.org/10.1038/nrm934>
- Tokhunts, R., S. Singh, T. Chu, G. D'Angelo, V. Baubet, J.A. Goetz, Z. Huang, Z. Yuan, M. Ascano, Y. Zavros, et al. 2010. The full-length unprocessed hedgehog protein is an active signaling molecule. *J. Biol. Chem.* 285: 2562–2568. <https://doi.org/10.1074/jbc.M109.078626>
- Tulin, S., and A. Stathopoulos. 2010. Analysis of Thisbe and Pyramus functional domains reveals evidence for cleavage of *Drosophila* FGFs. *BMC Dev. Biol.* 10:83–100. <https://doi.org/10.1186/1471-213X-10-83>
- Wharton, K.A., and M. Serpe. 2013. Fine-tuned shuttles for bone morphogenetic proteins. *Curr. Opin. Genet. Dev.* 23:374–384. <https://doi.org/10.1016/j.gde.2013.04.012>